# Numerical modelling of the interaction between translatory waves and a ship during navigation lock filling

Louis Algoet

Supervisor: Prof. dr. ir. Tom De Mulder
Counsellors: Pedro Cunha Ramos, Thomas Boelens

Master's dissertation submitted in order to obtain the academic degree of
Master of Science in Civil Engineering

Department of Civil Engineering
Chair: Prof. dr. ir. Peter Troch
Faculty of Engineering and Architecture
Academic year 2016-2017

GHENT
UNIVERSITY

# Numerical modelling of the interaction between translatory waves and a ship during navigation lock filling

Louis Algoet

Supervisor: Prof. dr. ir. Tom De Mulder
Counsellors: Pedro Cunha Ramos, Thomas Boelens

Master's dissertation submitted in order to obtain the academic degree of
Master of Science in Civil Engineering

Department of Civil Engineering
Chair: Prof. dr. ir. Peter Troch
Faculty of Engineering and Architecture
Academic year 2016-2017

GHENT
UNIVERSITY

Ghent, August 2017

# Acknowledgement

This master's thesis is the result of a year of hard work and devotion. The completion of this work would not have been possible without the assistance and guidance of so many people whose names may not all be enumerated.

First and most of all, I would like to acknowledge my thesis supervisor, Professor dr. ir. Tom De Mulder of the Laboratory for Hydraulics of Ghent University. The door to Professor De Mulder's office was always open whenever I ran into difficulties or had a question about my research or writing. He consistently allowed this thesis to be my own work, yet steered me in the right direction whenever he thought I needed it.

I would also like to thank dr. ir. Laurent Schindfessel of the Laboratory for Hydraulics of Ghent University for making time to answer specific questions with respect to one of his research assignments I was allowed to use. In addition, I want to thank my counsellors Pedro Cunha and Thomas Boelens.

As this master's thesis concludes my studying period at the Ghent University, I wish to thank my friends and classmates for five extremely interesting years and the many beautiful moments we shared during our years of studying.

In particular, I would like to express my gratitude to Karen Allart, for her support and for providing me with the necessary distraction whenever I needed it. I am also gratefully indebted to her for her valuable comments after proofreading this work.

Finally, I want to thank my parents and my brother, not only for proofreading this work, but for their support and encouragement during the establishment of this work.

Louis Algoet,
Ghent, August 2017

**Numerical modelling of the interaction between translatory waves and a ship during navigation lock filling**

Author: Louis Algoet

Supervisor: Prof. dr. ir. Tom De Mulder
Counsellors: Pedro Cunha Ramos, Thomas Boelens

Master's dissertation submitted in order to obtain the academic degree of Master of Science in Civil Engineering

Department of Civil Engineering
Chair: Prof. dr. ir. Peter Troch
Faculty of Engineering and Architecture
Academic year 2016-2017

# Abstract

For this master's thesis, a MATLAB code is developped for modelling lock filling and emptying. The 1D SWE are applied to model the water movement, and both the flexible and the rigid ship method are implemented to model the presence of a moored vessel. For the solution of the applicable system of (partial) differential equations, two numerical solution methods are implemented.
After debugging the developped code, the obtained results are studied for the Denderbelle test case, for a lock chamber without a moored vessel. The sensitivity of the results to the numerical parameters for both numerical solution methods is studied, in order to select adequate values for these numerical parameters. For the selected numerical parameters, the results obtained with both solution methods are compared.
Finally, one possibility to increase the applicability of this one-dimensional model is studied, namely including representative profiles for the momentum correction coefficient β, in order to better represent the concentrated filling jet.

Keywords: navigation lock, translatory wave, longitudinal force on a moored vessel, Preissmann scheme, Runge-Kutta time-stepping, momentum correction coefficient

# Numerical modelling of the interaction between translatory waves and a ship during navigation lock filling

Author: Louis Algoet

Supervisor: Prof. dr. ir. Tom De Mulder

***Abstract* – In this master's thesis, a MATLAB code is developped for modelling lock filling and emptying. The 1D SWE are applied to model the water movement, and both the flexible and the rigid ship approaches are implemented to model the presence of a moored vessel. For the solution of the applicable system of (partial) differential equations, two numerical solution methods are implemented. The influence of the obtained results to the numerical solution method is then studied for the Denderbelle lock. Finally, one possibility to increase the applicability of this one-dimensional model is studied, namely including representative profiles for the momentum correction coefficient β, in order to better represent the concentrated filling jet.**

***Keywords* – navigation lock, translatory wave, longitudinal force on a moored vessel, Preissmann scheme, Runge-Kutta time-stepping, momentum correction coefficient**

## I. INTRODUCTION

Navigation locks are key structures for navigation in canals and canalized rivers, as well as for the accessibility of ports. The design of an adequate filling and emptying system is crucial within the overall design of a navigation lock, and influences the design of many of the other elements to be constructed. The two most important design criteria with respect to F/E systems deal with limitations on the time required for F/E, and on the acting forces on the moored vessels.

For the estimation of the longitudinal forces on a moored vessel, numerical models are often applied, especially during the conceptual design. In this master's thesis, a MATLAB code is developped, applying the one-dimensional shallow water equations (1D SWE) to model the water movement, and both the flexible and rigid ship method to account for the presence of a moored vessel. Two numerical solution methods are implemented to solve the resulting system of (partial) differential equations, so that the influence of the numerical solution method can be studied.

Finally, the influence of incorporating representative profiles for the momentum correction coefficient β is studied, with the aim to better represent the concentrated filling jet in this one-dimensional model.

## II. MATHEMATICAL FORMULATION OF LOCK FILLING AND EMPTYING

For the developped code 'Lock_Filling.m', the water movement is modelled by applying the 1D SWE. The following formulation of the shallow water equations is considered (applicable to a lock chamber without a moored vessel)

$$\begin{cases} B_c \dfrac{\partial h}{\partial t} + \dfrac{\partial Q}{\partial x} = 0 \\ \dfrac{\partial Q}{\partial t} + \dfrac{\partial}{\partial x}\left(\dfrac{\beta Q^2}{A}\right) + gA\dfrac{\partial h}{\partial x} + g\dfrac{Q|Q|}{C^2AR} = 0 \end{cases}$$

with

| | |
|---|---|
| $B_c$ | lock chamber width [m] |
| h | water level deviation [m] (with respect to $h_0$) |
| Q | discharge [$m^3/s$] |
| β | momentum correction coefficient [-] |
| A | wet cross sectional area [$m^2$] |
| R | hydraulic radius [m] |
| C | Chézy friction coefficient [$m^{0.5}/s$] |
| g | acceleration due to gravity [$m/s^2$] |
| $h_0$ | initial water level in the lock chamber [mREF] |

To account for the presence of a moored vessel, both the flexible and the rigid ship approaches are implemented.

For the flexible ship approach, the ship is assumed to be able to flexibly follow the water movement at any point along its length. For the section with the flexible ship, the applicable system of partial differential equations is the same as the one described above. The presence of the moored ship is represented by the adjusted geometrical characteristics.

For the rigid ship approach, the ship is modelled as a rigid box. The water movement during lock filling then results in a certain sinkage s and pitch γ of the ship. These effects apply at the midship's cross section. The system of partial differential equations to be solved for the section with the rigid ship differs from the one described above. The continuity equation contains two extra terms, and two additional second order ordinary differential equations have to be solved to determine the unkown sinkage s and pitch γ after each time step.

## III. NUMERICAL SOLUTION METHOD

For the solution of the applicable system of (partial) differential equations, two numerical solution methods are implemented in 'Lock_Filling.m'. The first is based on the modified Stelling (1978) method by De Mulder [1]. For this method, the applicable system of (partial) differential equations is rewritten to express the time derivatives on the left-hand side, as a function of the other terms on the right-hand side. Central finite difference approximations are applied for the partial derivatives with respect to space. Since only the spatial derivatives are discretized, this approach is indicated as semi-discretization. The Runge-Kutta 4$^{th}$ order time-stepping method is then applied to solve for the unkown dependent variables at the next time step.

The second implemented numerical solution method is the space-centered Preissmann scheme. Both the space and time derivatives are approximated with central finite differences, applying a weighting factor θ in time. The resulting system of non-linear discretized equations is solved iteratively by applying the Newton-Raphson algorithm. Since a system of non-linear equations has to be solved iteratively for each time step, the required calculation time increases significantly.

## IV. SENSITIVITY ANALYSIS

Before studying the influence of including representative profiles for the momentum correction coefficient, the sensitivity of the results to the numerical parameters for both implemented solution methods is studied.

Even though a lock chamber without a moored vessel is simulated, the results for the bow-to-stern slope are studied since this slope is typically used to estimate the longitudinal force on the moored vessel. Because the distance between the bow and the upstream lock gate is 5 m, the spatial step Δx is taken equal to 2.5 m, and is not further adjusted for this master's thesis.

In Fig. 1, the bow-to-stern slope is displayed for different values for the time step Δt for the modified Stelling (1978) method. The parameter $t_{niv,2}$ denotes the instant in time where the absolute value of the difference between the equilibrium water level $h_e$, and the average water level in the lock chamber is smaller than 1 mm. No significant differences in the results are observed for the bow-to-stern slope when varying the time step Δt before $t_{niv,2}$ is reached. Furthermore, it is observed that the variation of the bow-to-stern slope corresponds to the typical variation expected for the longitudinal force component due to the translatory wave effect (mainly positive values before the maximum discharge is reached, and mainly negative values afterwards). However, when the time step is increased (from 0.20 s onwards), the bow-to-stern slope does not approach zero for longer simulation times as expected. To that end, a sufficiently small time step Δt equal to 0.01 s is selected.

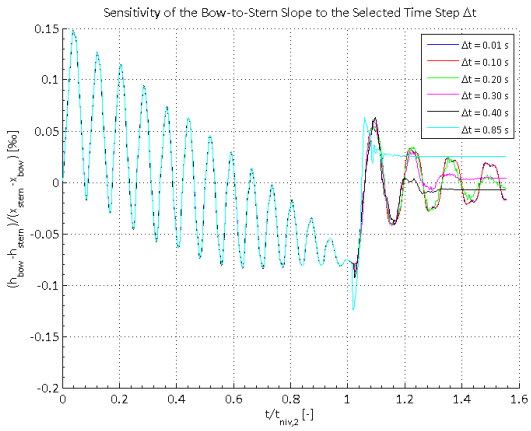


Fig. 1 – Sensitivity of the bow-to-stern slope to Δt for the modified Stelling (1978) method

In Fig. 2, the bow-to-stern slope is displayed for different values for the time step Δt for the Preissmann method. The same remarks for the variation of the bow-to-stern slope before $t_{niv,2}$ is reached can be made as for Fig. 1. For the Preissmann method, the bow-to-stern slope is observed to oscillate towards zero for longer simulation times. Furthermore it is noted that by increasing the time step (and as such the CFL number), the numerical damping also increases. For the first three time steps, the results correspond well with each other. Therefore, a time step Δt equal to 0.50 s is selected. For the higher time steps, the increased numerical damping becomes more pronounced. The selected time steps corresponds to CFL numbers in the neighbourhood of 1.0 as also recommended in [2].

Fig. 3 displays the bow-to-stern slope for different values of the weighting factor θ in time (for the selected time step Δt). As expected, increasing the parameter θ between 0.5 and 0.7 leads to an increase of the numerical damping. To that end, a value of

0.55 is selected for reasons of accuracy, as also proposed in [2].

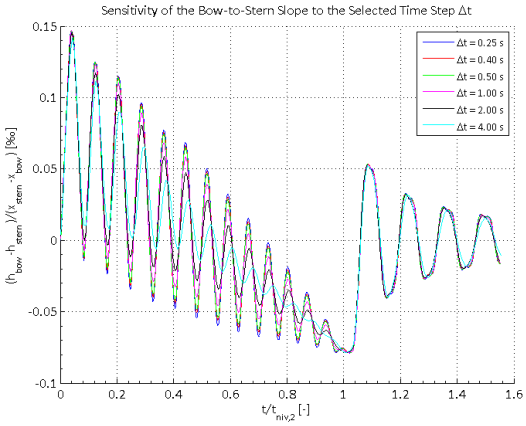


Fig. 2 – Sensitivity of the bow-to-stern slope to Δt for the Preissmann method

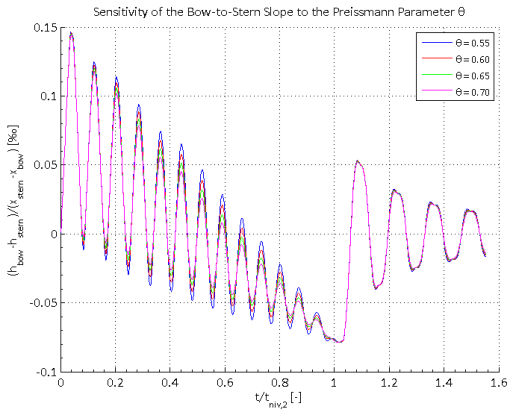


Fig. 3 – Sensitivity of the bow-to-stern slope to θ for the Preissmann method

In Fig. 4 the obtained results for the bow-to-stern slope are compared for the modified Stelling (1978) and the Preissmann method (for the selected numerical parameters).

From Fig. 4, some differences can be observed between the results obtained with both methods. Especially with respect to the downward peaks, the modified Stelling (1978) method seems to display lower peaks.

Finally, the large difference in the required calculation time is mentioned here, respectively 96 s and 42.88 s for the modified Stelling (1978) and the Preissmann method. This huge difference is attributed to the necessity to solve a system of non-linear equations for each time step for the Preissmann method. The code for the Preissmann method should be further optimized.

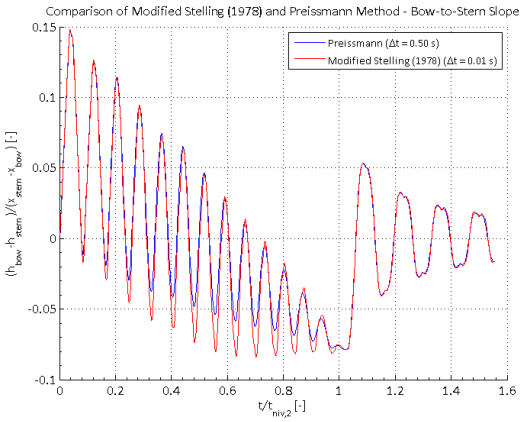


Fig. 4 – Comparison of the bow-to-stern slope for the modified Stelling (1978) and the Preissmann method

## V. INFLUENCE OF THE MOMENTUM CORRECTION COEFFICIENT

Finally, the influence of including representative profiles for the momentum correction coefficient β is studied. These profiles are determined based on the output of the provided MATLAB routine 'vul_sluis_impuls_straal_LVH.m' [3].

For the Preissmann method, including this routine leads to a tremendous increase in the required calculation time (order of magnitude of weeks). Therefore only the modified Stelling (1978) method is studied with respect to including the momentum correction coefficient.

In Fig. 5, the bow-to-stern slope is displayed for the modified Stelling (1978) method (for the selected time step Δt), both for the simulation where β is equal to 1.0 and for β determined based on the output of the routine 'vul_sluis_impuls_straal_LVH.m'.

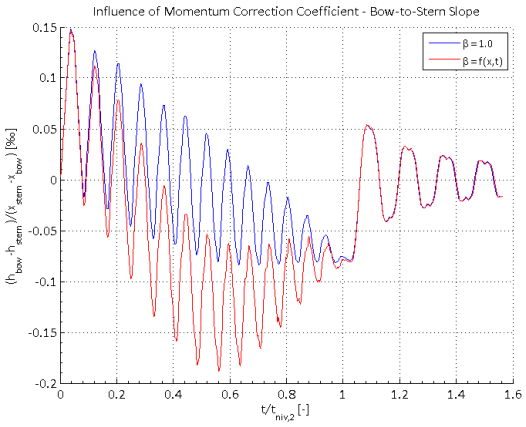


Fig. 5 – Influence of the momentum correction coefficient on the bow-to-stern slope for the modified Stelling (1978) method

When the momentum correction coefficient is included, the oscillatory behaviour attributed to the translatory wave effect is still observed, yet the overall curve also displays a downwards deflection (and a corresponding minimum value). This typical variation of the bow-to-stern slope corresponds to the variation of the longitudinal force component on a moored vessel due to both the translatory wave and the momentum decrease effects.

## VI. CONCLUSION

By including representative profiles for the momentum correction coefficient β, the variation of the bow-to-stern slope corresponds to the typical variation of the longitudinal force component due to both the translatory wave and the momentum decrease effects. Including the momentum correction coefficient can therefore further enhance the applicability of the 1D SWE by better representing the concentrated filling jet.

Further research is recommended in order to determine which longitudinal force components (calculated separately in LOCKFILL and 'vul_sluis.m') are inherently represented by applying the 1D SWE, especially with respect to the translatory wave and the momentum decrease effects. It is proposed to study the expression for the longitudinal force component due to the momentum decrease along the length of the vessel, as implemented in LOCKFILL and 'vul_sluis.m'. The obtained results with the for this master's thesis developped code 'Lock_Filling.m' can also be compared to the results obtained with LOCKFILL and 'vul_sluis.m'.

## VII. REFERENCES


[1] T. De Mulder, *Modified Stelling (1978) approach to solve 1D Shallow Water Equations in a lock chamber. Documentation of Fortran code,* 2006.

[2] G. A. Schohl, User's Manual for LOCKSIM, Norris, Tennessee: TVA Engineering Laboratory, 1998.

[3] L. Schindfessel and T. De Mulder, "Memo studieopdracht naar de berekening van debiet en impuls in het programma vul_sluis.m [in Dutch]," Hydraulics Laboratory, Dep. Civil Engineering, Ghent University, Ghent, 2017.

# Table of Contents

# List of Figures

# List of Tables

# List of Symbols

| | |
|---|---|
| $F_{x,transl}$ | longitudinal force component due to translatory waves [‰] |
| $h_{bow}$ | water level deviation at the bow of the moored vessel [m] |
| $h_{stern}$ | water level deviation at the stern of the moored vessel [m] |
| $L_s$ | length of the vessel [m] |
| $C_b$ | block coefficient of the vessel [-] |
| h | water level deviation w.r.t. the initial water level in the lock chamber $h_0$ [m] |
| g | acceleration due to gravity [$m/s^2$] |
| $A_c$ | wet cross sectional area of the lock chamber [$m^2$] |
| $A_s$ | cross sectional area of the vessel [$m^2$] |
| Q | discharge [$m^3/s$] |
| C | Chézy friction coefficient [$m^{0.5}/s$] |
| R | hydraulic radius [m] |
| B | width at the water line [m] |
| β | momentum correction coefficient [-] |
| A | wet cross sectional area [$m^2$] |
| $S_0$ | bed slope [-] |
| $S_f$ | friction or energy slope [-] |
| $h_e$ | equilibrium water level in the lock chamber [mREF] |
| $h_0$ | initial water level in the lock chamber [mREF] |
| $h_b$ | level of the lock chamber bottom [mREF] |
| $B_s$ | beam of the vessel [m] |
| $T_s$ | draft of the vessel [m] |
| $B_c$ | width of the lock chamber [m] |
| P | wetted perimeter [m] |
| $P_c$ | wetted perimeter of the lock chamber [m] |
| $R_c$ | hydraulic radius of the lock chamber [m] |
| $k_c$ | roughness length of the lock chamber walls (and bottom) [m] |
| $P_s$ | wetted perimeter of the vessel [m] |
| s | sinkage of the vessel [m] |
| γ | pitch of the vessel [rad] |
| $x_M$ | distance between the midship's cross section and the upstream lock gate [m] |
| $V_s$ | displacement volume of the vessel [$m^3$] |
| $x_{bow}$ | distance between the bow and the upstream lock gate [m] |
| $x_{stern}$ | distance between the stern and the upstream lock gate [m] |
| $\alpha_1$ | auxiliary variable for the determination of s [m/s] |
| $\alpha_2$ | auxiliary variable for the determination of γ [rad/s] |
| $L_c$ | lock chamber length [m] |
| μ(t) | discharge coefficient at time t [-] |
| $A_{opening}(t)$ | open area for the gate opening at time t [$m^2$] |
| $h_{gate}$ | water level deviation just downstream of the upstream lock gate [m] |
| Δt | time step [s] |

| | |
|---|---|
| $\Delta x$ | spatial step [m] |
| $N_q$ | number of discharge nodes for the modified Stelling (1978) method [-] |
| $N_h$ | number of water level nodes for the modified Stelling (1978) method [-] |
| $N_t$ | number of time steps [-] |
| $\sigma$ | Courant-Friedrichs-Lewy (CFL) number [-] |
| $N_x$ | number of nodes for the Preissmann method [-] |
| $\theta$ | weighting factor in time for the Preissmann scheme [-] |
| $\phi$ | weighting factor in space for the Preissmann scheme [-] |
| d | numerical damping [-] |
| $c_r$ | numerical dispersion [-] |
| $v_{lift}$ | lift velocity of the vertical lift valves [m/s] |
| $h_{valve}(t)$ | lifted valve height as a function of time [m] |
| $\theta(t)$ | relative lift height of the valves as a function of time [-] |
| $b_{opening}$ | width of the gate opening(s) [m] |
| $h_{opening}$ | height of the gate opening(s) [m] |
| U | cross sectional averaged velocity [m/s] |
| $Q_{max}$ | maximum filling discharge [$m^3/s$] |
| $h_{avg}$ | average water level in the lock chamber [mREF] |
| D | vertical length scale [m] |
| L | horizontal length scale [m] |
| T | time scale [s] |
| Fr | Froude number [-] |
| $U_0$ | velocity scale [m/s] |

# 1. Introduction

Navigation locks are key structures for navigation in canals and canalized rivers, as well as for the accessibility of ports. The design of an adequate filling and emptying system is crucial within the overall design of a navigation lock, and influences the design of many of the other elements to be constructed. The two most important design criteria with respect to F/E systems deal with limitations on the time required for F/E and on the acting forces on the moored vessels.

In general F/E systems can be subdivided into two main categories. For relatively high lifts ( [1] mentions 15 metres and more) longitudinal culvert systems are typically applied. For lower lifts ( [1] mentions lifts up to 6 metres) through the heads filling systems are mostly adopted. The denotation 'through the heads' indicates that the lock is filled or emptied either through short culverts in the lock heads bypassing the gate, or through openings in the gates.

In Belgium, the lift height for most inland navigation locks is limited to about 2 to 3 metres. For this range of lift heights, through the heads F/E through openings in the gates is often considered [2]. When filling through openings in the gates, the concentrated jet leads to a zone of very turbulent water near the lock head. This disturbed zone then spreads through the whole lock chamber (Figure 1). This is particularly disadvantageous with respect to the forces acting on vessels moored in the lock chamber [1].

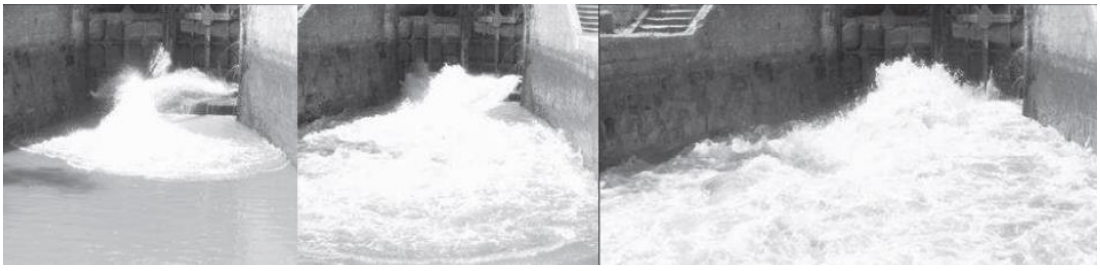

**Figure 1 – Zone of turbulent water when filling through openings in the gates [1]**

During the preliminary design, numerical packages are typically used for comparing different F/E systems and conditions, with respect to the filling time and the acting longitudinal forces on moored vessels. The three-dimensional flow pattern arising during lock filling or emptying (as observed in Figure 1), would imply the use of three-dimensional Computational Fluid Dynamics (3D CFD) codes, solving the Reynolds-Averaged Navier-Stokes (RANS) equations. These models still require huge computational efforts and skilled operators, which are not always readily available. Furthermore it is noted that most CFD codes were developped for internal flow problems, and some extra challenges might have to be overcome when modelling problems involving free surface flows [3].

Simplified methods have been proposed and studied for modelling lock filling and emptying for different through the heads F/E systems. In LOCKFILL [4] and 'vul_sluis.m' [5], the sloshing of the water level in the lock chamber during F/E is determined by the superposition of many small translatory waves, generated by the non-constant flow rate through the gate openings. For the determination of

the longitudinal component of the force on the ship, each of the contributing components is calculated separately, and the results are superimposed.

In LOCKSIM [6] and Stelling (1978) [7], the one-dimensional shallow water equations (1D SWE) are used to describe the water movement in the lock chamber. Depending on how the moored vessel is modelled, these equations are appropriately adjusted to account for the presence of the ship, and additional equations are added. Applying this one-dimensional approach to a clearly three-dimensional problem (Figure 1) is quite a significant simplification. One possibility to further enhance the applicability of the 1D SWE models could be to include the momentum correction coefficient to better represent the velocity profiles due to the filling jet.

For this master's thesis, lock filling and emptying through openings in the gates will be numerically modelled by solving the one-dimensional shallow water equations, applying two different discretization methods. On the one hand, the modified Stelling (1978) method is reprogrammed, and on the other hand the classical Preissmann scheme is implemented. The obtained results are then used to quantify the acting forces due to translatory waves on a vessel moored in the lock chamber. The influence of including appropriate profiles for the momentum correction coefficient is studied as well.

Since the acting hawser forces are generally lower during emptying the lock chamber (since the energy dissipation takes place outside the lock chamber), in this master's thesis only the situation of lock filling will be simulated further on. The code written for this master's thesis will be referred to as 'Lock_Filling.m'.

# 2. Hawser Forces During Filling of a Navigation Lock

The term 'hawser forces' indicates the forces exerted on the hawsers or mooring lines of a moored vessel[1]. During lock filling, different external forces attempt to displace a moored vessel from its initial position. The hawser forces can be interpreted as the reaction forces in the mooring lines opposing this movement.

The above definition for the term 'hawser forces' is only useful when the forces are determined based on models incorporating the real mooring lines system. However, during the conceptual design of a F/E system, the hawser forces are typically estimated numerically, based on software solving the 1D (e.g. Stelling (1978) and LOCKSIM) or 2D SWE, or applying other simplified methods to describe the water movement in the lock chamber (e.g. LOCKFILL, 'vul_sluis.m'). These models typically do not include a representation of the mooring lines system. In the design phase, the hawser forces are typically determined based on physical scale model tests. Modelling the real configuration of mooring lines would lead to technical problems so that often these are not modelled. Therefore, in [8] multiple definitions for the term 'hawser forces' are described, mainly depending on the adopted approach for their practical determination. For a detailed overview of these definitions, the reader is referred to the mentioned paper.

In this master's thesis, the 1D SWE will be applied to describe the water movement in the navigation lock during filling. Therefore, the term 'hawser forces' refers to the hydrostatic forces exerted on the hull of the vessel [8]. The resultant of these hydrostatic forces (divided by the vessel's displacement weight) will be approximated by the slope of the water surface between the bow and the stern of the moored vessel.

For the evaluation of the design of a F/E system, the estimated hawser forces obtained from numerical or physical model tests are compared with a certain threshold value. The applicable hawser force criterion imposes quite some demands on the design of the F/E system, in order to avoid damage to the lock structure or the vessel due to uncontrolled vessel movement and/or rupture of mooring lines. Typically the hawser forces are expressed as a permillage of the ship's displacement weight. For inland navigation vessels, standard hawser force threshold values are put forward by international (e.g. PIANC) or national authorities.

In general, the hawser forces consist of both a longitudinal and a transversal component. By applying a one-dimensional model, the transversal hawser force component can not be estimated. This limitation does not restrict the use of these 1D SWE models (especially during the conceptual design), since the longitudinal component is typically dominant for through the heads F/E systems.

The same sign convention for the longitudinal hawser force component as applied in LOCKFILL [4] and 'vul_sluis.m' [5] is adopted. This sign convention is displayed in Figure 2, and indicates that the forces are positive when directed away from the lock head through which filling or emptying takes place.

[1] Hawser is a nautical term for a thick cable or rope used in mooring or towing a ship [22].

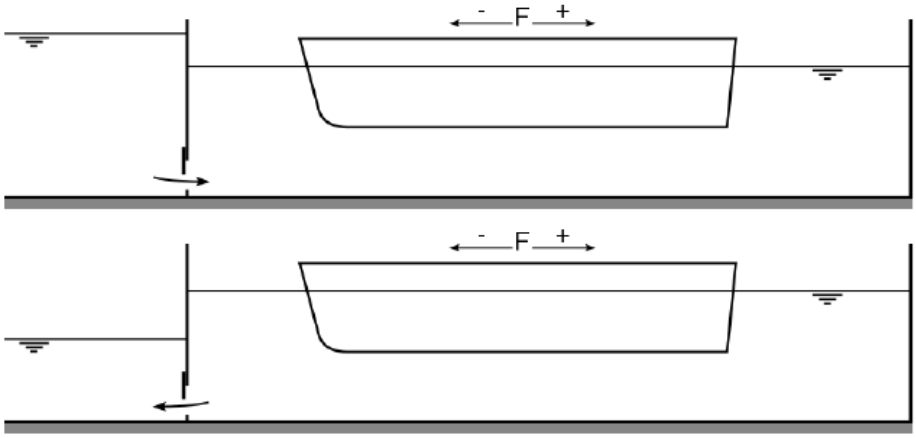


**Figure 2 – Sign convention for the longitudinal force during lock filling (top) or emptying (bottom) [4]**

In LOCKFILL, the longitudinal force on the moored vessel is determined based on the contributions of five different components [4]. A brief description of these five components is provided in the following since this provides useful physical insight. As noted before, LOCKFILL does not model the water movement by solving the 1D SWE. It is noted here that the differentiation of the longitudinal force into these five components is less straightforward when solving the 1D SWE, since it is not immediately clear which components are inherently included by applying this system of equations. Following the description of each of the components, some remarks are made with respect to this issue.

For the case of lock filling, the different components are displayed schematically in Figure 3. Their description below follows the same notation as the one in Figure 3.

a.) Translatory waves

Translatory waves are generated by the non-constant filling discharge through the openings in the gates. These translatory waves travel back and forth in the lock chamber, where complete reflection against the lock gates, and partial reflection against the bow and the stern of the vessel are typically assumed. The result is an oscillating motion of the water in the lock chamber (sloshing), generating an oscillating force on the moored vessel.

In LOCKFILL, the force component due to translatory waves, dimensionless with respect to the vessel's displacement weight, is determined based on the water level difference between the bow and the stern of the vessel

$$F_{x,transl} = \frac{h_{bow} - h_{stern}}{L_s C_b}$$

Due to the way the water movement is modelled in LOCKFILL, this force component has to be compensated for damping afterwards.

In [5] the local value for the longitudinal slope of the water surface in a section with ship is rewritten based on derived expressions for the translatory wave amplitude and celerity. The slope of the water surface in a section with ship is then written as

$$\frac{\partial h}{\partial x} = \frac{1}{g(A_c - A_s)} \frac{\partial Q}{\partial t}$$

For the derivation of this expression, it is assumed that the ship is able to flexibly follow the water movement (i.e. the flexible ship approach). The flexible and rigid ship approaches will be described in paragraphs 3.1.2.1 and 3.1.2.2 respectively.

In [5] it is noted that this last expression for the slope of the water surface is a strongly simplified form of the more general expression proposed by Bosma (1978)

$$\frac{\partial h}{\partial x} = \frac{1}{g(A_c - A_s)} \left( \frac{\partial Q}{\partial t} + \frac{\partial}{\partial x} \left( \frac{Q^2}{(A_c - A_s)} \right) + g \frac{Q|Q|}{C^2 (A_c - A_s) R} \right)$$

This last expression is a formulation for the momentum equation of the 1D SWE, rearranged to express the slope of the water surface as a function of the other terms. It is clear that in LOCKFILL, the advection and friction terms are not immediately considered, which explains the necessity to compensate for damping afterwards. For this master's thesis, the 1D SWE are applied to model the water movement, so that the effects of the advection and friction terms are automatically included when determining the water level differences between the bow and the stern of the vessel.

b.) Momentum decrease over the length of the vessel

In [4], the longitudinal hawser force component due to the momentum decrease over the length of the vessel is described as the combination of two effects. Firstly, when filling through openings in the gates, the concentrated filling jet leads to high flow velocities that decrease in the longitudinal direction. Secondly, the average flow rate decreases in the longitudinal direction for each cross section, since behind each cross section, a smaller part of the lock chamber has to be filled. These effects cause a total decrease of the momentum in the longitudinal direction, which results in water level differences between the bow and stern of the vessel, and a corresponding longitudinal force.

In LOCKFILL expressions are provided to determine this longitudinal force component When applying a 1D SWE approach, the decrease of the discharge in the longitudinal direction is represented. However the modelling of the filling jet still poses some challenges in most numerical packages. In this master's thesis, the influence of including a momentum correction coefficient to represent the non-uniform velocity profiles of the filling jet is studied. It is expected that the decrease of the flow velocities in the longitudinal direction is then also represented, so that the calculated water level difference between the bow and the stern of the vessel, and the as such estimated longitudinal hawser force component, will include both the translatory wave as the momentum decrease effects. These two effects typically contribute the most to the total longitudinal force on the moored vessel.

c.) Friction

The friction of the flow with the hull of the vessel exerts a friction force on the moored vessel. Furthermore, the frictional losses of the flow with the hull of the vessel and with the lock chamber walls and bottom, have an influence on the water level difference between the bow and the stern of the vessel.

The friction force on the hull of the vessel will have to be calculated separately for the 1D SWE approach, but by including the friction term in the 1D SWE, the effect of the frictional losses on the water level differences between the bow and the stern of the moored vessel is included. The friction force exerted on the hull of the moored vessel is not considered in this master's thesis.

d.) Direct filling flow against the bow

Depending on the position and the height of the gate openings above the lock bottom, the effect of the direct filling jet onto the bow of the moored vessel has to be considered. In LOCKFILL, this force component is calculated by determining the flow pressure against a plate under an angle. In this master's thesis, this force component is not studied.

The force component due to the direct impact of the filling jet is typically present in the beginning of the levelling process. When the ship has risen high enough, the jet is able to pass under the ship, and the force component disappears.

e.) Density differences over the length of the vessel

For the sake of completeness, the effect of density differences is also mentioned. A density difference (e.g. due to salinity differences) between the water in the lock chamber and the water in the upper reach will induce the formation of density currents in the lock chamber. As these density currents travel through the lock chamber, reflecting against the bow and the stern of the moored vessel and against the lock gates, this gives rise to water level differences in the longitudinal direction. In LOCKFILL, this effect is implemented but is not available in the public release. In this master's thesis, the effect of density differences will not be implemented or studied.

In LOCKFILL, the total longitudinal force is obtained by adding all of the separately determined contributions. For most navigation lock designs, the translatory wave and the momentum decrease components are observed to contribute the most to the total longitudinal hawser force. These components are therefore studied further in this master's thesis.

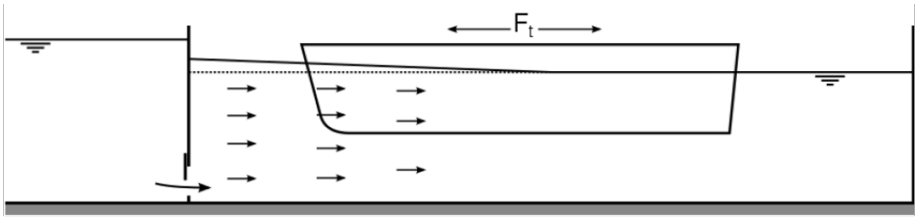


(a) Translatory waves

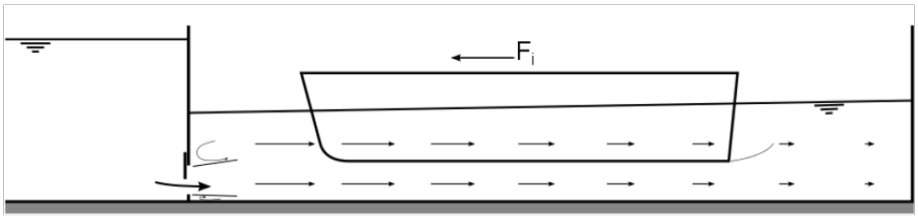


(b) Momentum decrease over the length of the vessel

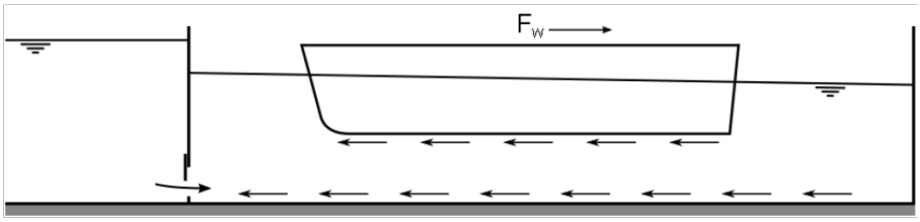


(c) Friction

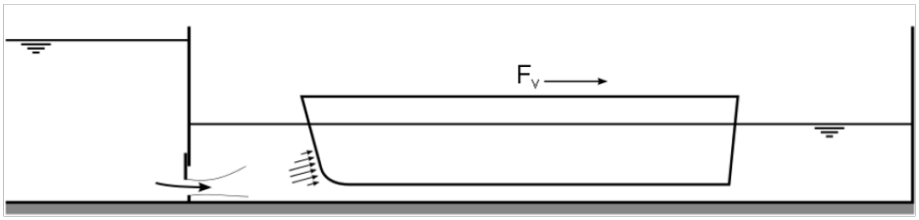


(d) Direct filling flow against the bow

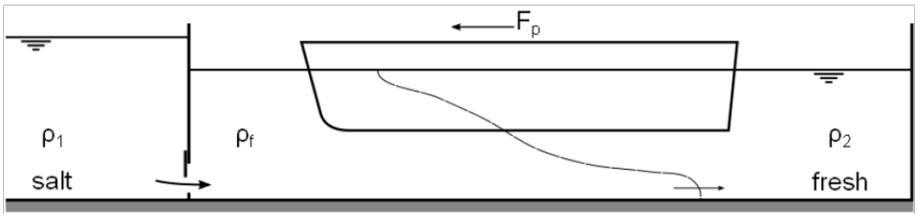


(e) Density differences over the length of the vessel

**Figure 3 – Longitudinal force components on a moored vessel during lock filling [4]**

# 3. Mathematical Formulation of Lock Filling and Emptying

For this master's thesis, the one-dimensional shallow water equations (1D SWE) are applied to model the water movement in the lock chamber during filling and emptying. These one-dimensional shallow water equations (also frequently referred to as the one-dimensional Saint-Venant equations) describe the time-varying flow in open channels with fixed bottom. The term shallow water equations indicates that they apply to flow problems in open channels where the vertical length scale (water depth) is much smaller than the horizontal length scale.

For a 1D formulation, two dependent variables suffice to describe the time-varying flow. These dependent variables are function of the two independent variables, namely the space coordinate x along the channel's length, and the time coordinate t. For the problem of lock filling or emptying, the water level deviation h and the discharge Q are selected as the dependent variables.

To determine the variation of the dependent variables with respect to the independent variables, the system of 1D SWE, consisting of a continuity and a momentum equation, is solved. In literature, many different formulations for the 1D SWE can be found. In this master's thesis, the formulation as described in [9] is adopted, since this formulation is easily modified to the system of equations proposed in [7], and applied later on. The system of 1D SWE becomes

$$\begin{cases} B\dfrac{\partial h}{\partial t} + \dfrac{\partial Q}{\partial x} = 0 \\ \dfrac{\partial Q}{\partial t} + \dfrac{\partial}{\partial x}\left(\dfrac{\beta Q^2}{A}\right) = gA\left(S_0 - S_f - \cos(\theta)\dfrac{\partial h}{\partial x}\right) \end{cases}$$

Before applying this system of equations, the underlying assumptions are summarized, to be able to verify the applicability to the problem of lock filling and emptying. The following assumptions apply for the system of 1D SWE as described above

- the water density $\rho_w$ is constant,
- the flow varies gradually, i.e. there are no large values for the slope of the water surface (discontinuities in the water surface),
- the vertical accelerations (centrifugal accelerations) are negligible, requiring that the streamlines are only gently curved in the vertical plane, so that the channel's cross sections can be assumed hydrostatic,
- the velocities are perpendicular to the cross sections (due to the 1D approach)
- the open channel is prismatic
- there is no lateral inflow/outflow in the open channel.

For the problem of lock filling or emptying, these assumptions are more or less satisfied. Since the contribution of density currents to the hawser forces is not modelled, the density of the water is assumed to be constant. Translatory waves are generated during filling and emptying the lock chamber, and these waves are characterized as long waves. This justifies the assumption of gradually varying flow and gently curved streamlines in the vertical plane. The assumption that the velocities are

perpendicular to the channel's cross sections is a simplification inherent to the one-dimensional model for the case of lock filling and emptying (as displayed in Figure 1). The lock chamber cross section can typically be simplified to be prismatic without large errors. Finally, no lateral inflow/outflow is considered for this master's thesis, yet minor adjustments can be made to include for these effects.

To determine the relative importance of the different terms in the momentum equation, a dimensional analysis is described in Appendix A. From this dimensional analysis, it follows that the most important terms are the local acceleration and the pressure gradient term, and that the friction term and the advective acceleration term are of lesser importance. For the indication of these terms, reference is made to Appendix A.

In the following sections, an overview of the systems of (partial) differential equations to be solved for the different implemented cases is provided. Special care is devoted to the description of the geometrical characteristics for each of the different situations.

A mathematically complete formulation of a physical problem not only requires the description of the applicable (partial) differential equations, but also the specification of the initial and boundary conditions. These are therefore also included in this paragraph.

## 3.1. Differential Equations

In this paragraph, a subdivision is made between a lock chamber without a moored vessel, and a lock chamber with a moored vessel[2]. Figure 4 displays a simplified sketch of the general case of a lock chamber with a moored vessel during lock filling, and the different sections to be distinguished.

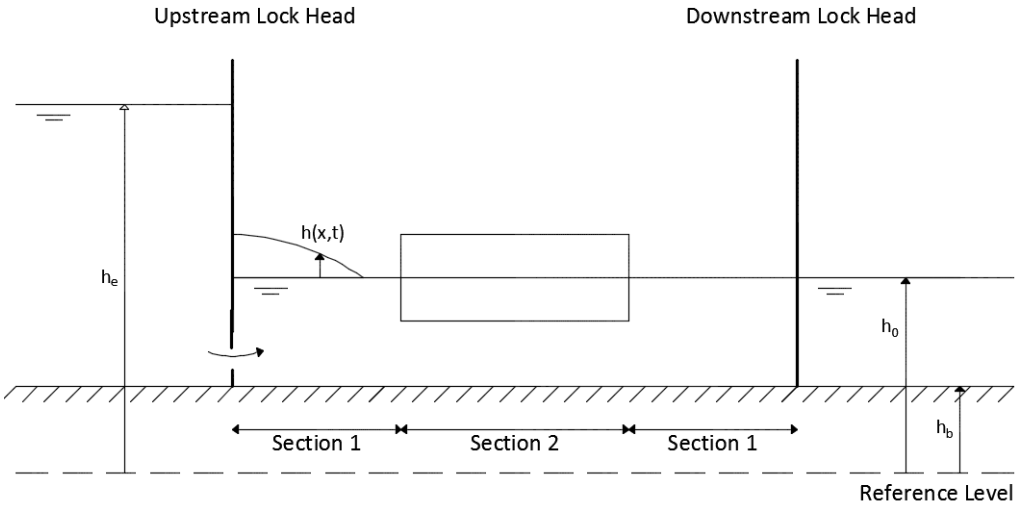


**Figure 4 – General sketch of a simplified lock chamber with a moored vessel during filling**

[2] In 'Lock_Filling.m', the presence of a moored vessel can be toggled on and off by setting the flag 'i_ship' respectively equal to one and zero.

From Figure 4, it is clear that the lock chamber bottom is assumed to be horizontal. It is also noted that the water levels $h_0$ and $h_e$ are expressed relative to the selected reference level. The dependent variable h(x,t) represents the deviation in the water level with respect to the initial water level in the lock chamber (i.e. $h_0$). The lock chamber is assumed to have a prismatic shape with a rectangular cross section. The ship will be simplified to a rectangular box with dimensions $L_s$, $B_s$ and $T_s$, and both the flexible and the rigid ship approach will be implemented, as described further on.

### 3.1.1. Lock Chamber Without Moored Vessel

Firstly, the system of equations to be solved for filling or emptying a lock chamber without a moored vessel is described. This system of equations also applies to the sections without ship in a lock chamber with a moored vessel (sections 1 in Figure 4). The following system of 1D SWE applies

$$\begin{cases} B_c \dfrac{\partial h}{\partial t} + \dfrac{\partial Q}{\partial x} = 0 \\ \dfrac{\partial Q}{\partial t} + \dfrac{\partial}{\partial x}\left(\dfrac{\beta Q^2}{A}\right) + gA\dfrac{\partial h}{\partial x} + g\dfrac{Q|Q|}{C^2AR} = 0 \end{cases}$$

In this master's thesis the lock chamber bottom is assumed to be horizontal. The term representing the bed slope in the above described system of 1D SWE is then equal to zero ($S_0 = 0$).

For a lock chamber without a moored vessel, or the sections indicated with the number one in a lock chamber with a moored vessel, the wet cross sectional area, wetted perimeter and hydraulic radius are respectively determined as

$$A(x,t) = A_c(x,t) = B_c(h_0 + h(x,t) - h_b)$$

$$P(x,t) = P_c(x,t) = B_c + 2(h_0 + h(x,t) - h_b)$$

$$R(x,t) = R_c(x,t) = \frac{A(x,t)}{P(x,t)}$$

In the above expressions, the subscript 'c' stands for (lock) chamber.

In the formulation of the 1D SWE stated above, the friction slope $S_f$ is expressed with a Chézy formulation. Instead of specifying the Chézy coefficient as a constant input parameter, an expression for the Chézy coefficient is implemented based on the work of Thijsse [10]. The Chézy coefficient is determined as a function of the hydraulic radius R and the wall roughness $k_c$, and assuming a hydraulic rough wall as follows

$$C(x,t) = 18\log_{10}\left(\frac{12R(x,t)}{k_c}\right)$$

In [10] it is noted that in the Netherlands, experience has shown that this expression gives sufficiently correct results for closed as well as for open channels. No specific restrictions for the application of this formula are mentioned.

### 3.1.2. Lock Chamber With Moored Vessel

Secondly, the system of (partial) differential equations to be solved in the sections with ship (indicated as section 2 in Figure 4) is described. Two different methods are implemented for modelling the moored vessel, the flexible and the rigid ship method[3]. These methods mainly differ in their way of describing the influence of the presence of the moored ship on the propagation of the translatory waves in the lock chamber.

#### 3.1.2.1. Flexible Ship Method

For the flexible ship method, the ship is assumed to be able to flexibly follow the water movement at any point along its length, and by doing so adopts the shape of the generated translatory waves. This is schematically displayed in Figure 5.

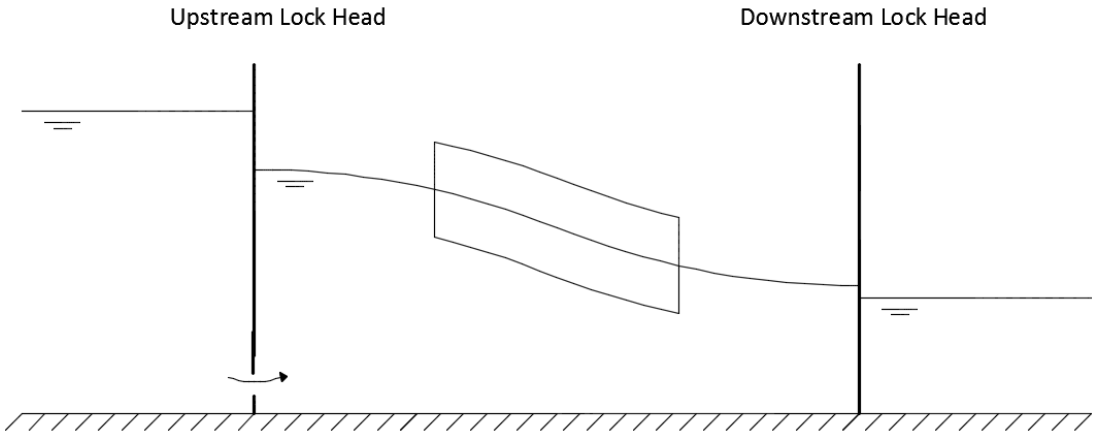


**Figure 5 – Simplified sketch for the principle of the flexible ship method**

A first consequence of the ship flexibly following the water movement, is that at every location along its length, the draft remains equal to the initially specified draft $T_s$. A second consequence is that the translatory waves are able to travel over the entire width of the lock chamber in the sections with ship. The system of equations to be solved in the section with ship (section 2 in Figure 4) is then identical to the one in the sections without ship, as described in the previous paragraph. For the sake of completeness this system of equations is repeated here

[3] In 'Lock_Filling.m' the flexible or the rigid ship method can be selected by setting the flag 'i_rigid' respectively equal to zero and one.

$$\begin{cases} B_c \dfrac{\partial h}{\partial t} + \dfrac{\partial Q}{\partial x} = 0 \\ \dfrac{\partial Q}{\partial t} + \dfrac{\partial}{\partial x}\left(\dfrac{\beta Q^2}{A}\right) + gA\dfrac{\partial h}{\partial x} + g\dfrac{Q|Q|}{C^2AR} = 0 \end{cases}$$

The presence of the ship becomes clear from the determination of the geometrical characteristics. For the ship modelled as a flexible ship, the wet cross sectional area, wetted perimeter and hydraulic radius respectively become

$$A(x,t) = A_c(x,t) - A_s(x,t) = B_c(h_0 + h(x,t) - h_b) - B_s T_s$$

$$P(x,t) = P_c(x,t) + P_s(x,t) = B_c + 2(h_0 + h(x,t) - h_b) + B_s + 2T_s$$

$$R(x,t) = \frac{A(x,t)}{P(x,t)}$$

The Chézy friction coefficient is again calculated as

$$C(x,t) = 18\log_{10}\left(\frac{12R(x,t)}{k_c}\right)$$

The remark is made that the hydraulic radius is determined based on the wet cross sectional area and the wetted perimeter of both the lock chamber and the moored vessel. The expression for the Chézy friction coefficient then applies the lock chamber wall roughness $k_c$ to the perimeter of the vessel as well, even though the lock chamber walls and the ship's hull are clearly constructed from different materials. This formulation for the Chézy friction coefficient is nevertheless used throughout this master's thesis both for the sections without and the section with ship. This is partly justified by the fact that the friction term is of lesser importance compared to the local acceleration and pressure gradient terms (following the dimensional analysis conducted in Appendix A).

#### 3.1.2.2. Rigid Ship Method

For the rigid ship method, the vessel is modelled as a rigid box. The translatory waves generated during filling and emptying the lock chamber lead to a certain sinkage s and pitch γ. These parameters apply at the vessel's midship's cross section. This is displayed in Figure 6, together with the adopted sign convention.

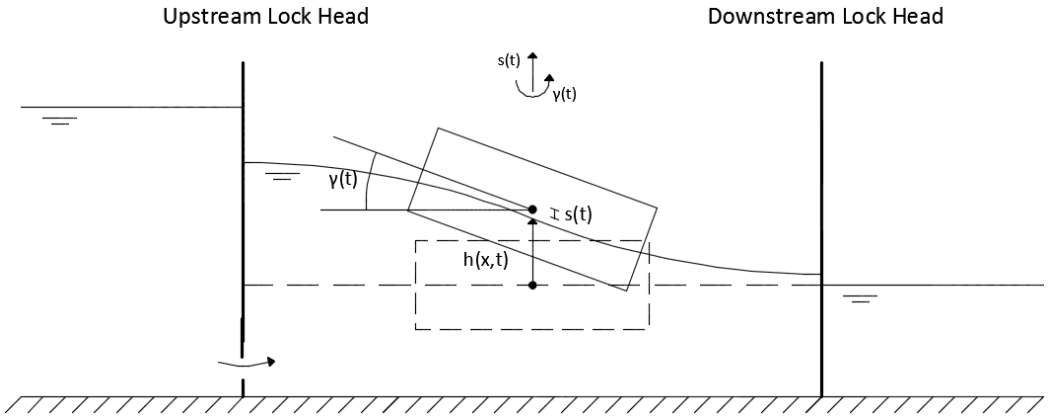


**Figure 6 – Simplified sketch for the principle of the rigid ship method**

The sinkage s and the pitch γ for the ship modelled as a rigid box require the solution of two ordinary second order differential equations additional to the partial differential equations constituting the 1D SWE. When modelling the ship as rigid, the continuity equation is adjusted, and contains two extra terms. The system of equations to be solved in the section with ship becomes [7]

$$\begin{cases} (B_c - B_s)\dfrac{\partial h}{\partial t} + \dfrac{\partial Q}{\partial x} = -B_s\dfrac{ds}{dt} - B_s(x - x_M)\dfrac{d\gamma}{dt} \\ \dfrac{\partial Q}{\partial t} + \dfrac{\partial}{\partial x}\left(\dfrac{\beta Q^2}{A}\right) + gA\dfrac{\partial h}{\partial x} + g\dfrac{Q|Q|}{C^2AR} = 0 \\ \dfrac{d^2s}{dt^2} + \dfrac{2gB_s}{V_s}\dfrac{L_s}{2}s = \dfrac{gB_s}{V_s}\displaystyle\int_{x_{bow}}^{x_{stern}} h dx \\ \dfrac{d^2\gamma}{dt^2} + \dfrac{2gB_s}{V_s}\dfrac{L_s}{2}\gamma = \dfrac{3gB_s}{V_s\left(\frac{L_s}{2}\right)^2}\displaystyle\int_{x_{bow}}^{x_{stern}} h(x - x_M)dx \end{cases}$$

The above system of (partial) differential equations is rewritten by defining two auxiliary variables $\alpha_1$ and $\alpha_2$. The second order ordinary differential equations then become first order ordinary differential equations with respect to these auxiliary variables, and two additional first order ordinary differential equations have to be solved to determine the sinkage s and pitch γ from the defined auxiliary variables. Eventually, this leads to the following system of equations

$$\begin{cases} (B_c - B_s)\dfrac{\partial h}{\partial t} + \dfrac{\partial Q}{\partial x} = -B_s\alpha_1 - B_s(x - x_M)\alpha_2 \\ \dfrac{\partial Q}{\partial t} + \dfrac{\partial}{\partial x}\left(\dfrac{\beta Q^2}{A}\right) + gA\dfrac{\partial h}{\partial x} + g\dfrac{Q|Q|}{C^2AR} = 0 \\ \dfrac{d\alpha_1}{dt} + \dfrac{gB_sL_s}{V_s}s = \dfrac{gB_s}{V_s}\displaystyle\int_{x_{bow}}^{x_{stern}} h dx \\ \dfrac{d\alpha_2}{dt} + \dfrac{gB_sL_s}{V_s}\gamma = \dfrac{12gB_s}{V_sL_s^2}\displaystyle\int_{x_{bow}}^{x_{stern}} h(x - x_M)dx \\ \dfrac{ds}{dt} = \alpha_1 \\ \dfrac{d\gamma}{dt} = \alpha_2 \end{cases}$$

The difference between the flexible and rigid ship methods also becomes clear from the determination of the geometrical characteristics. For the rigid ship method, the draft is not constant along the length of the vessel as is the case for the flexible ship method. The wet cross sectional area, the wetted perimeter and the hydraulic radius become

$$A(x,t) = B_c(h_0 + h(x,t) - h_b) - B_s(x)\big(T_s(x) - s(t) - \gamma(t)(x - x_M) + h(x,t)\big)$$

$$P(x,t) = B_c + 2(h_0 + h(x,t) - h_b) + B_s(x) + 2\big(T_s(x) - s(t) - \gamma(t)(x - x_M) + h(x,t)\big)$$

$$R(x,t) = \frac{A(x,t)}{P(x,t)}$$

The Chézy friction coefficient is calculated using the same formula as mentioned in the previous paragraphs

$$C(x,t) = 18\log_{10}\left(\frac{12R(x,t)}{k_c}\right)$$

The same remark with respect to the applicability of this formula in a section with ship as the one described for the flexible ship method can be made here.

## 3.2. Initial Conditions

Since the systems of (partial) differential equations are solved over a finite time interval, initial conditions are required to describe the influence of the (pre)history onto the problem.

For this master's thesis only lock filling will be studied since the resulting hawser forces are higher compared to when the lock chamber is being emptied. The initial water level in the lock chamber $h_0$ is

then equal to the water level of the downstream reach. The water in the lock chamber is assumed to be completely at rest before the valves are opened to start the levelling process. The initial conditions for the dependent variables h and Q are then

$$h(x,0) = 0\ m$$

$$Q(x,0) = 0\ \frac{m^3}{s}$$

When the ship is modelled using the rigid ship method, initial conditions have to be specified for the auxiliary variables $\alpha_1$ and $\alpha_2$ and for the sinkage s and pitch γ as well. Initially, the ship rests in a horizontal position with a constant draft along its length, so that the initial conditions are specified as

$$\alpha_1(0) = 0$$

$$\alpha_2(0) = 0$$

$$s(0) = 0$$

$$\gamma(0) = 0$$

## 3.3. Boundary Conditions

Since the systems of (partial) differential equations are solved in a limited spatial domain, boundary conditions are required to describe the influence of the exterior space.

Only first order spatial derivatives of the dependent variables h and Q occur. For each of the dependent variables, one boundary condition has to be specified. From the theory of characteristics it follows that for subcritical flow, as is the case for lock filling, these boundary conditions have to be specified at opposite boundaries [9].

To model the levelling process of a navigation lock, both boundary conditions are easily expressed for the dependent variable Q. The downstream lock gate is modelled as a closed boundary during filling, so that

$$Q(L_c,t) = 0\ \frac{m^3}{s}$$

For the filling discharge, a Bernoulli equation is written along a streamline from the upper reach to the lock chamber. The filling discharge can then be determined as

$$Q(0,t) = \mu(t)A_{opening}(t)\sqrt{2g\left|h_e - \left(h_0 + h_{gate}\right)\right|}sign\left(h_e - \left(h_0 + h_{gate}\right)\right)$$

For this master's thesis, the upper reach is assumed to be infinitely large, so that the water level of the upper reach (i.e. $h_e$) remains constant. As observed in the above equation, the head as a function of time is calculated based on the water level difference between the upper reach $h_e$ and the water level just downstream of the upstream lock gate.

# 4. Modified Stelling (1978) Method

In [7], G.S. Stelling describes and studies a mathematical model for describing the water and ship movement in a navigation lock during filling or emptying. This mathematical model consists of the 1D SWE to describe the water movement, and two ordinary second order differential equations to describe the ship movement (rigid ship method as described in paragraph 3.1.2.2). G.S. Stelling studies both a classical finite difference method, and the method of lines, and compares these two methods with respect to their accuracy, stability, and efficiency.

Prof. T. De Mulder developped a FORTRAN code [11], for the G.S. Stelling method of lines approach, albeit with a different time-stepping method to advance the system of first order differential equations, namely the 4$^{th}$ order Runge-Kutta time-stepping method. This method is further referred to as the modified Stelling (1978) method, and is reprogrammed in MATLAB for this master's thesis.

In this paragraph, the most important aspects of the modified Stelling (1978) method are outlined. For more details, specifically with respect to the implementation in MATLAB, the reader is referred to Appendix B.

## 4.1. Grid

For the modified Stelling (1978) approach, the grid is staggered in space (but not in time). The applied grid is displayed in Figure 7.

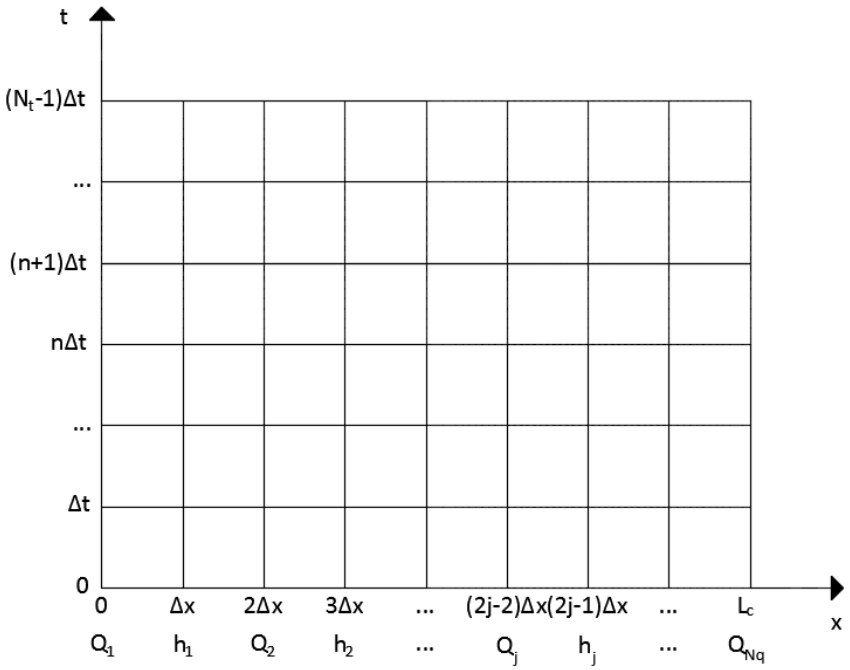


**Figure 7 – Space staggered grid for the modified Stelling (1978) method**

From Figure 7 it is clear that the grid is constructed in such a way that both boundaries coincide with discharge nodes. This complies with the specified boundary conditions described in paragraph 3.3.

The choice for a staggered grid typically gives rise to some additional difficulties during programming. For example, positioning the ship in the lock chamber becomes somewhat more tedious, and requires special attention (Appendix B). One of the reasons that could explain the choice for a staggered grid over a collocated grid, is that the numerical problem of spurious oscillations that sometimes occurs when applying a collocated grid is avoided by applying a staggered grid. For more information with respect to this issue, reference is made to [12] and [13].

## 4.2. Discretization in Space

For the modified Stelling (1978) method, the systems of (partial) differential equations are rewritten to express the partial derivatives with respect to time on the left-hand side, as a function of the other terms on the right-hand side for each of the (partial) differential equations to be solved. For the system of (partial) differential equations applicable to a section containing a rigid ship, this becomes

$$\begin{cases} \dfrac{\partial h}{\partial t} = \dfrac{1}{B_c - B_s}\left[-\dfrac{\partial Q}{\partial x} - B_s\alpha_1 - B_s(x - x_M)\alpha_2\right] \\ \dfrac{\partial Q}{\partial t} = -\dfrac{\partial}{\partial x}\left(\dfrac{\beta Q^2}{A}\right) - gA\dfrac{\partial h}{\partial x} - g\dfrac{Q|Q|}{C^2AR} \\ \dfrac{d\alpha_1}{dt} = -\dfrac{gB_sL_s}{V_s}s + \dfrac{gB_s}{V_s}\displaystyle\int_{x_{bow}}^{x_{stern}} h dx \\ \dfrac{d\alpha_2}{dt} = -\dfrac{gB_sL_s}{V_s}\gamma + \dfrac{12gB_s}{V_sL_s^2}\displaystyle\int_{x_{bow}}^{x_{stern}} h(x - x_M)dx \\ \dfrac{ds}{dt} = \alpha_1 \\ \dfrac{d\gamma}{dt} = \alpha_2 \end{cases}$$

In order to apply the Runge-Kutta 4th order time-stepping method, only the terms on the right-hand side of the above system of (partial) differential equations are discretized. With respect to the derivatives, this corresponds to only discretizing the partial derivatives with respect to space. This is denoted as semi-discretization.

In this paragraph, the applied finite difference approximations for the different terms are described in general. The systems of discretized (partial) differential equations are presented in Appendix B. In the next paragraph, the Runge-Kutta 4th order time-stepping method is discussed.

For the discretization of the partial derivatives with respect to space, central difference schemes are applied. For the partial derivative of the discharge with respect to the space coordinate x occuring in the continuity equation, this becomes

$$\left(\frac{\partial Q}{\partial x}\right)_{h_j} \approx \frac{Q_{j+1} - Q_j}{2\Delta x}$$

The subscript $h_j$ indicates that the central difference scheme is applied with respect to the point $h_j$. Similar central difference schemes are applied to the advection and pressure gradient terms of the momentum equation, following the modified Stelling (1978) approach [11]. It is important to note that this differs from the applied Leap frog finite difference scheme, in combination with the angled derivative method for the discretization of the advection term, as proposed by G.S. Stelling [7].

The truncation error for the applied central difference scheme is obtained by writing Taylor series expansions. In [9], this is done for the central difference scheme. Since the leading term in the truncation error is of the order of $\Delta x^2$, the applied central difference scheme is said to be second order accurate in space. In short, this is notated as $O(\Delta x^2)$.

No special measures were taken for the discretization of the non-linear friction term. The discretization of this term is performed as follows for the discharge node $Q_j$

$$\left(-g\frac{Q|Q|}{C^2AR}\right)_{Q_j} \approx -g\frac{Q_j|Q_j|}{\left(\frac{C_{j-1}+C_j}{2}\right)^2\left(\frac{A_{j-1}+A_j}{2}\right)\left(\frac{R_{j-1}+R_j}{2}\right)}$$

Since the geometrical characteristics are only calculated at water level nodes, linear interpolation is required to determine these geometrical characteristics and Chézy friction coefficients at the discharge nodes.

The integrals occuring in the ordinary differential equations for the determination of s and γ are approximated by applying Simpson's rule. The approximation of these integrals is described in Appendix B, since this depends on the way the ship is positioned in the lock chamber.

For the sections with and without ship, for both the flexible and the rigid ship method, the systems of discretized (partial) differential equations are presented in Appendix B.

## 4.3. Runge-Kutta 4th Order Time-Stepping Method

For the solution of the obtained system of semi-discretized (partial) differential equations, the Runge-Kutta 4th order time-stepping method is applied in the modified Stelling (1978) approach by De Mulder [11]. The RK4 method belongs to the family referred to as the Runge-Kutta schemes. The 4th order Runge-Kutta scheme is typically the most popular in literature, since it provides a good balance between accuracy, and computational effort.

In this paragraph, the RK4 method is described, applied to the practical problem of filling a lock chamber with a moored vessel, modelled according to the rigid ship method.

When the number of discharge nodes is equal to $N_q$, and the number of water level nodes is equal to $N_h$, the values of the dependent variables after n time steps are arranged in a column vector as follows

$$Y^n = \begin{bmatrix} Q_1^n \\ \vdots \\ Q_{N_q}^n \\ h_1^n \\ \vdots \\ h_{N_h}^n \\ \alpha^n \\ \beta^n \\ s^n \\ \gamma^n \end{bmatrix}$$

Due to the staggering in space, the number of discharge nodes $N_q$ is one more than the number of water level nodes $N_h$. The definition of the grid and the determination of $N_q$ and $N_h$ are extensively described in Appendix B.

Runge-Kutta time-stepping methods generally apply to differential equations written in the form

$$\frac{dy}{dt} = f(t, y)$$

where the variable y is a function of time. For the problem of lock filling, a column vector of dependent variables, each a function of time has to be approximated. The applicable discretized system of differential equations can then be written as

$$\frac{\partial Y}{\partial t} = F(t, Y)$$

where Y is the column vector of dependent variables (each a function of time), and F the column vector containing the discretized right-hand sides of the (partial) derivatives with respect to time for the different dependent variables.

The initial conditions as described in paragraph 3.2 are stored in the column vector $Y^0$. For the discharges at the boundary nodes, the partial derivatives with respect to time are set equal to zero, since these discharges are determined based on the applicable boundary conditions.

By applying the RK4 time-stepping method, the unkown values for the dependent variables at the next instant in time $Y^{n+1}$ are determined as

$$Y^{n+1} = Y^n + \frac{\Delta t}{6}(k_1 + 2k_2 + 2k_3 + k_4)$$

based on the known values at the current instant in time $Y^n$. In this expression, the parameters $k_1$, $k_2$, $k_3$ and $k_4$ are determined as follows

$$k_1 = F(t^n, Y^n)$$

$$k_2 = F\left(t^n + \frac{\Delta t}{2}, Y^n + k_1 \frac{\Delta t}{2}\right)$$

$$k_3 = F\left(t^n + \frac{\Delta t}{2}, Y^n + k_2 \frac{\Delta t}{2}\right)$$

$$k_4 = F(t^{n+1}, Y^n + k_3 \Delta t)$$

The column vector $k_1$ contains estimates for the slopes at the beginning of the time step. These slopes are then used to step halfway through the time step to calculate a first estimate of the slopes $k_2$ halfway through the time step. The slopes $k_2$ are then used to step halfway through the time step again, in order to get a second estimate for the slopes at the halfway point. Finally the slopes $k_3$ are used to step all the way across the time step to determine an estimate for the slopes $k_4$ at the end of the time step.

Weighting factors are assigned to each of the parameters $k_1$ to $k_4$, in order to achieve the desired order of accuracy for the approximation. These weighting factors are determined by solving a system of non-linear algebraic equations, obtained by specifying that certain terms in the Taylor series expansion have to cancel out. It is noted that the weighting factors for the estimates of the slopes $k_2$ and $k_3$ at the halfway point are higher compared to the weighting factors for the slopes at the end points.

The RK4 method is fourth order accurate in time. The accuracy of the applied numerical solution method for the modified Stelling (1978) method can then be notated in short as $O(\Delta t^4, \Delta x^2)$. The attentive reader notes the difference in the order of accuracy in time and in space, and questions why the RK4 method is selected over for example the RK2 method. This choice is mainly based on stability considerations.

The 1D SWE are a system of partial differential equations of the hyperbolic type. Semi-discretization by applying central difference schemes in space results in a system of ordinary discretized partial differential equations with eigenvalues in the neighbourhood of the imaginary axis [7]. Numerical solution methods with a stability region containing a large part of the imaginary axis are therefore preferable.

In [14] the stability regions for Runge-Kutta methods of orders one to four are visualized in the $\Omega\Delta t$ plane[4] (Figure 8).When comparing the stability regions for the RK2 and the RK4 method, it is clear that the RK4 method contains a large part of the imaginary axis (up to a value of $2\sqrt{2}$), whereas the RK2 method does not contain any part of the imaginary axis. These observations justify the choice of the RK4 over the RK2 method.

[4] The eigenvalue $\Omega\Delta t$ of a numerical problem depends on the equation(s) to be solved, the discretization scheme and the numerical solution method.

The stability region in the plane of the eigenvalues ΩΔt can be translated into a stability criterion for a specific problem. For a pure advection equation discretized using a central difference scheme, the eigenvalues are purely imaginary. When applying a RK4 numerical solution method, the imaginary part of the eigenvalues ΩΔt has to remain lower than the maximum allowable value for stability, equal to $2\sqrt{2}$. This criterion can typically be reformulated into a requirement with respect to the CFL number[5].

In literature, no explicit stability criterion is found for the specific case of the 1D SWE discretized in space using central difference schemes, solved by applying a RK4 time-stepping method. Nevertheless, the above observations for the pure advection problem are kept in mind.

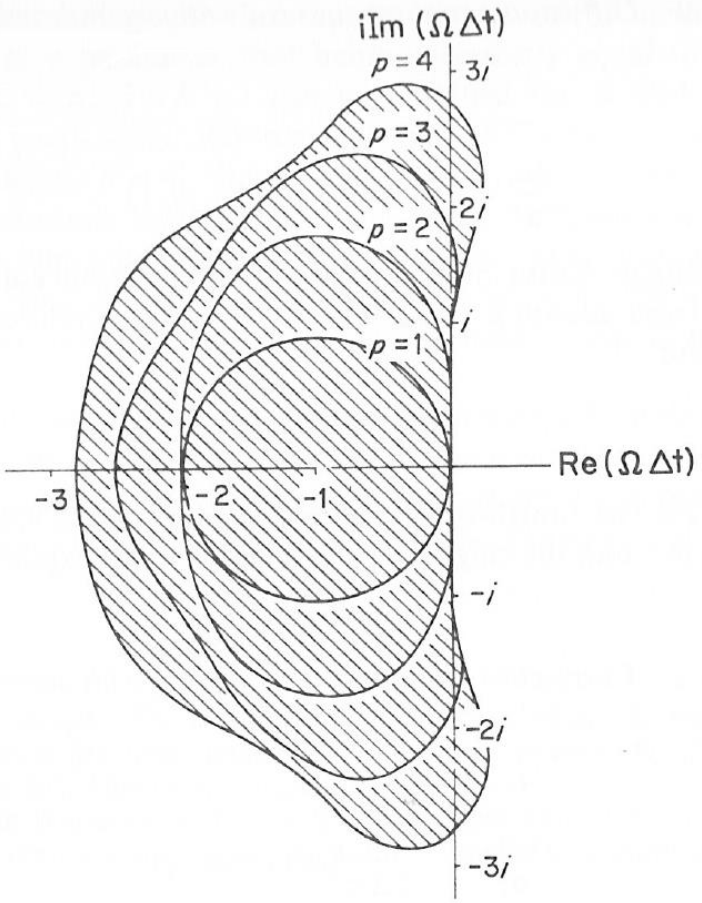


**Figure 8 – Stability regions for Runge-Kutta methods of orders 1, 2, 3 and 4 [14]**

[5] The CFL or Courant-Friedrichs-Lewy number (indicated as σ in this master's thesis) will be described further on.

# 5. Preissmann Method

For this master's thesis, a second finite difference method is also implemented in the MATLAB script 'Lock_Filling.m', for the numerical solution of the system of (partial) differential equations describing the water and the ship movement in a navigation lock during filling or emptying.

For this second finite difference method, the space centered four-point scheme, also commonly referred to as the space centered Preissmann scheme, or the box scheme is selected. In literature, many examples denote the popularity of this conventional Preissmann scheme, for the numerical solution of the 1D SWE. The popularity could be attributed to the unconditional stability of the Preissmann scheme applied to the 1D SWE, when the weighting factor θ lies between 0.5 and 1.0. The popularity can also be partly attributed to the compact molecule for the Preissmann scheme, that lends perfectly to the implementation of a variable spatial step Δx. This advantage may prove to be very useful for accurately positioning a moored vessel in the lock chamber.

## 5.1. Grid

For the implemented Preissmann scheme, a collocated grid is applied, as opposed to the space staggered grid selected for the modified Stelling (1978) method. The applied grid is displayed in Figure 9.

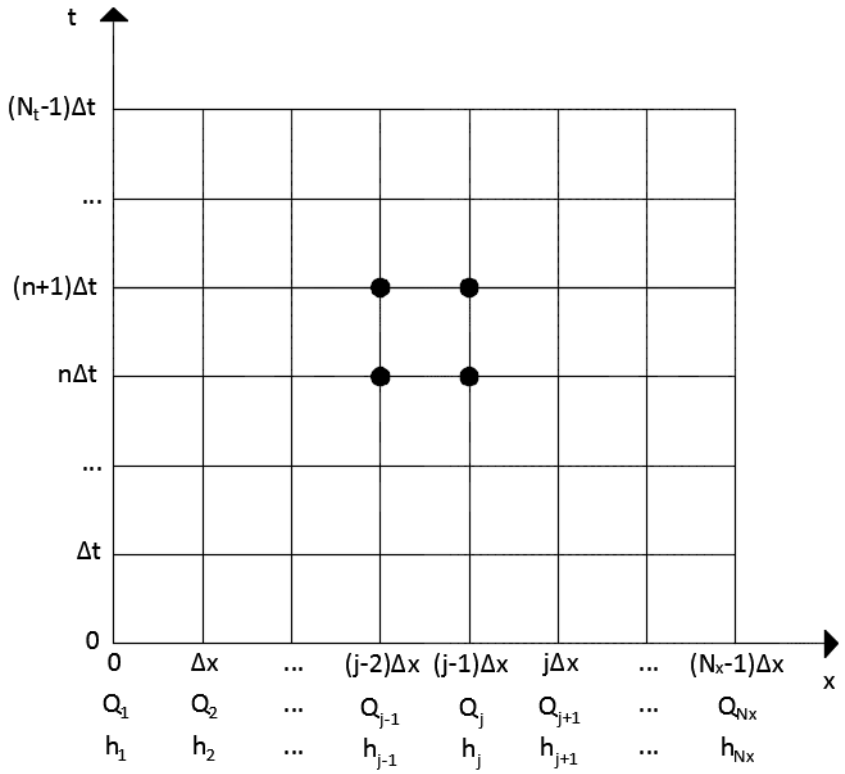


**Figure 9 – Collocated grid and molecule for the Preissmann method**

Considering the remark made with respect to the choice for a space staggered grid for the modified Stelling (1978) method, it is noted here that due to applying a collocated grid, the numerical solution might be susceptible to the numerical problem of spurious oscillations [12] and [13]. This is kept in mind when analyzing the results.

## 5.2. Discretization in Time and Space

To numerically solve the systems of (partial) differential equations as described in paragraph 3, the differential equations are discretized by applying finite difference approximations for both the time and spatial derivatives.

The approximation of the time derivatives for the most general description of the Preissmann scheme becomes

$$\frac{\partial h}{\partial t} \approx \frac{1}{\Delta t}\left[\phi\left(h_j^{n+1} - h_j^n\right) + (1-\phi)\left(h_{j-1}^{n+1} - h_{j-1}^n\right)\right]$$

In this expression, ϕ represents the weighting factor in space. For the here considered space centered scheme, ϕ is set equal to 0.5, and the finite difference approximation for the time derivatives becomes

$$\frac{\partial h}{\partial t} \approx \frac{1}{\Delta t}\left[0.5\left(h_j^{n+1} - h_j^n\right) + 0.5\left(h_{j-1}^{n+1} - h_{j-1}^n\right)\right] = \frac{1}{2\Delta t}\left[\left(h_j^{n+1} - h_j^n\right) + \left(h_{j-1}^{n+1} - h_{j-1}^n\right)\right]$$

The approximations for the spatial derivatives for the most general description of the Preissmann scheme becomes

$$\frac{\partial Q}{\partial x} \approx \frac{1}{\Delta x}\left[\theta\left(Q_j^{n+1} - Q_{j-1}^{n+1}\right) + (1-\theta)\left(Q_j^n - Q_{j-1}^n\right)\right]$$

The parameter θ represents the weighting factor in time. This parameter can be adjusted in the code 'Lock_Filling.m'.

For the dependent variables that do not occur as derivatives (e.g. the friction term, the integrals in the equations for the determination of the auxiliary variables $\alpha_1$ and $\alpha_2$, etc.), the following general approximation applies (illustrated for the discharge)

$$Q \approx \theta\left[\phi Q_j^{n+1} + (1-\phi)Q_{j-1}^{n+1}\right] + (1-\theta)\left[\phi Q_j^n + (1-\phi)Q_{j-1}^n\right]$$

For the space centered Preissmann scheme (i.e. ϕ = 0.5), this expression is simplified to

$$Q \approx \theta\left[\frac{Q_j^{n+1} + Q_{j-1}^{n+1}}{2}\right] + (1-\theta)\left[\frac{Q_j^n + Q_{j-1}^n}{2}\right] = \theta Q_{j-\frac{1}{2}}^{n+1} + (1-\theta)Q_{j-\frac{1}{2}}^n$$

Note the notation of the space centered quantities in the above approximation for the variable Q. This notation will be applied further on throughout this master's thesis.

Based on the described finite difference approximations, the systems of partial (and ordinary) differential equations described in paragraph 3 are discretized. For the sections with and without a moored vessel, and for both the flexible and the rigid ship method, the systems of discretized (partial) differential equations are presented in Appendix C.

In Figure 9, the molecule for the discretized 1D SWE for the Preissmann scheme is also displayed. Due to the typical form of this molecule, the space centered Preissmann scheme is also often referred to as the box scheme. As mentioned before, the compact form of the molecule for the Preissmann scheme lends perfectly to the implementation of a variable spatial step $\Delta x$. This could be very advantageous with respect to accurately positioning the ship in the numerical grid.

The Preissmann scheme is first order accurate in time, and second order accurate in space when the weighting factor $\theta$ differs from 0.5. This is notated in short as $O(\Delta t,\Delta x^2)$. For the special case where $\theta$ is equal to 0.5, the Preissmann scheme is second order accurate both in time and space, notated as $O(\Delta t^2,\Delta x^2)$. It is noted that the order of accuracy in time is lower compared to the one for the modified Stelling (1978) method.

The Preissmann scheme is unconditionally stable when the weighting factor $\theta$ lies between 0.5 and 1.0. In principle, this allows for the selection of a larger time step $\Delta t$ compared to the previously described modified Stelling (1978) method. An adequate choice for the time step $\Delta t$ has to be made, considering the accuracy of the numerical solution. The numerical damping and dispersion for the Preissmann scheme are respectively displayed in Figure 10 and Figure 11 as a function of the time step $\Delta t$ relative to the applicable wave period T. No numerical damping or diffusion occur when the parameters d and $c_r$ are equal to one.

From Figure 10 and Figure 11 it is clear that the numerical damping and diffusion increase with increasing the time step $\Delta t$. For a constant spatial step $\Delta x$ this also corresponds to increasing the CFL number $\sigma$. It is also observed that by increasing the weighting factor $\theta$ for the Preissmann scheme, more numerical damping and diffusion are added.

The remark is made here that Figure 10 and Figure 11 are based on an available expression for the amplification factor $\rho$ for a pure advection equation, discretized by applying the space centered Preissmann scheme [14]. Nevertheless, these observations provide useful insights for making appropriate choices for the numerical parameters of the Preissmann scheme (as discussed in paragraph 8.1.2).

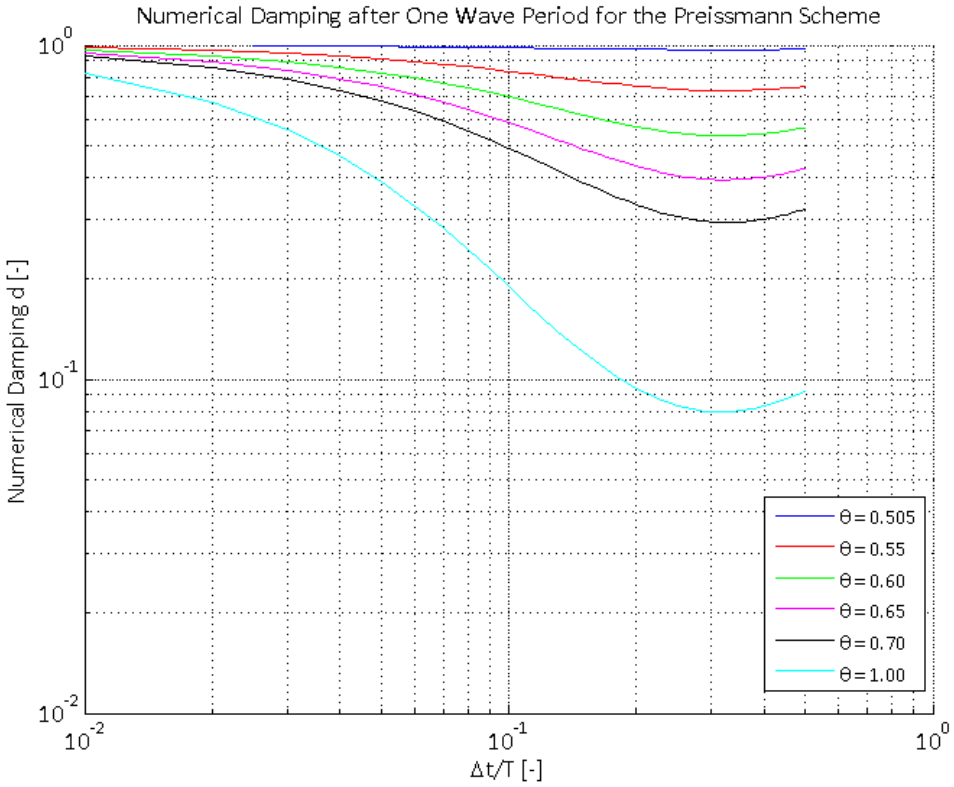


**Figure 10 – Numerical damping after one wave period for the space-centered Preissmann scheme**

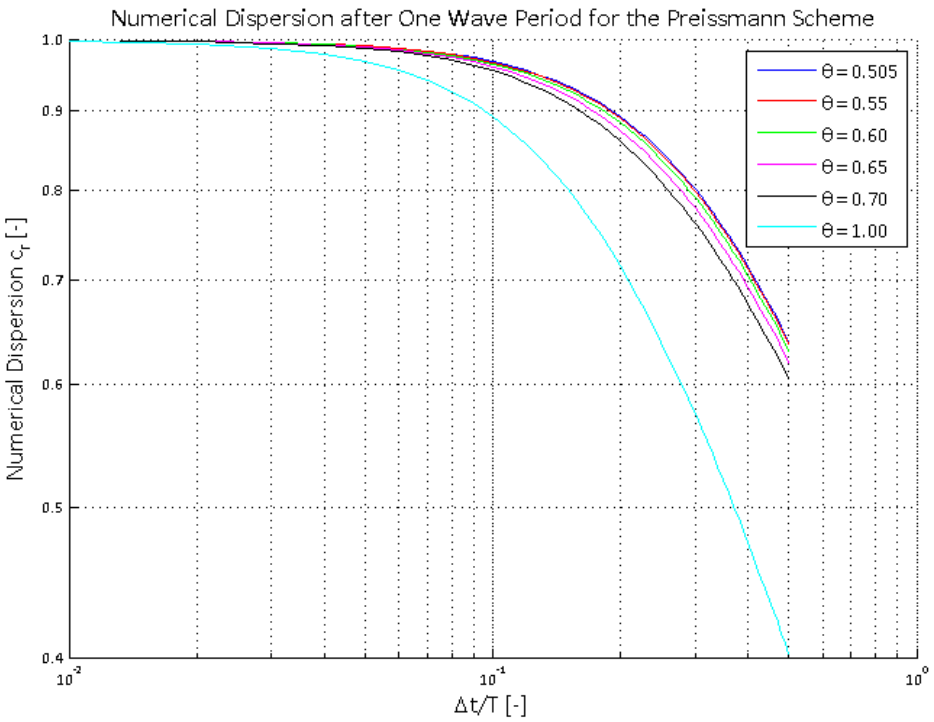


**Figure 11 – Numerical dispersion after one wave period for the space-centered Preissmann scheme**

## 5.3. Solution of the System of Discretized Partial Differential Equations

By applying the finite difference approximations described in the previous paragraph, the applicable system of (partial) differential equations is discretized. By incorporating the advection term and the Chézy formulation for the frictional effects, the resulting system of discretized equations is non-linear. The solution of this system of discretized equations is described in this paragraph based on the general approach outlined in [15].

The Newton-Raphson iterative solution technique is selected to solve the non-linear system of discretized equations. This algorithm provides an efficient means of converging to a solution, given a sufficiently good initial guess. It is noted here that there are countless other algorithms for solving such a system of non-linear equations.

For each time step, two unkown dependent variables (i.e. h and Q) have to be determined at each of the $N_x$ nodes, corresponding to $2N_x$ unkowns. To solve for these unkowns, $2N_x$ equations are required. For each of the $N_x$-1 cells, a continuity and momentum equation can be written. Together with the applicable boundary conditions at the up- and the downstream lock gate, this leads to a system of $2N_x$ equations. When the ship is modelled according to the rigid ship method, four additional unkowns and four additional equations have to be added to determine the values for the auxiliary variables $\alpha_1$ and $\alpha_2$ and for the sinkage s and the pitch γ at the ship's midship's cross section. In the following, each of these equations is represented by a shorter notation $F_i$

$$F_i(\vec{x}) = 0$$

with $\vec{x}$ the vector of unkown dependent variables

$$\vec{x} = \left(Q_1^{n+1}, h_1^{n+1}, \dots, Q_{j-1}^{n+1}, h_{j-1}^{n+1}, Q_j^{n+1}, h_j^{n+1}, \dots, Q_{N_x}^{n+1}, h_{N_x}^{n+1}\right)$$

For the equations $F_i$, the index i ranges from 1 to $2N_x$. For i equal to 1 respectively $2N_x$, $F_i$ represents the up- and downstream boundary conditions. For i ranging from 2 to $2N_x$-1, $F_i$ represents a continuity equation when the index is even, and a momentum equation when the index is uneven (for each of the $N_x$-1 cells).

For applying the Newton-Raphson iterative method, each of the functions $F_i$ is expanded in the neighbourhood of $\vec{x}$ as follows

$$F_i(\vec{x} + \delta\vec{x}) = F_i(\vec{x}) + \sum_{j=1}^{2N_x} \frac{\partial F_i}{\partial x_j} \delta x_j + O(\delta\vec{x}^2)$$

The above equations can be written in matrix form as

$$\vec{F}(\vec{x} + \delta\vec{x}) = \vec{F}(\vec{x}) + \vec{J} \cdot \delta\vec{x} + O(\delta\vec{x}^2)$$

where $\vec{F}$ denotes the column vector of functions $F_i$ and $\vec{J}$ the jacobian matrix of the system of non-linear equations. The column vector $\delta\vec{x}$ contains the corrections to the previous estimates for the solution of the non-linear system of equations after a certain number of time steps.

By setting the left-hand side equal to zero (in order to find the roots of the system of non-linear equations), and by neglecting the higher order terms, the above system of equations is simplified to

$$\vec{J} \cdot \delta\vec{x} = -\vec{F}(\vec{x})$$

The Jacobian matrix $\vec{J}$ contains the derivatives of the equations $F_i$ with respect to the unkown dependent variables. This matrix is displayed below. Note that the notation $F_i$ is replaced by UB, DB, $C_i$ and $M_i$ respectively for representing the up- and downstream boundary conditions, and the continuity and momentum equations for cell i.

$$\begin{bmatrix}
\frac{\partial UB}{\partial Q_1} & \frac{\partial UB}{\partial h_1} & 0 & 0 & 0 & 0 & 0 & 0 & 0 & 0 \\
\frac{\partial C_1}{\partial Q_1} & \frac{\partial C_1}{\partial h_1} & \frac{\partial C_1}{\partial Q_2} & \frac{\partial C_1}{\partial h_2} & 0 & \cdots & 0 & 0 & 0 & 0 \\
\frac{\partial M_1}{\partial Q_1} & \frac{\partial M_1}{\partial h_1} & \frac{\partial M_1}{\partial Q_2} & \frac{\partial M_1}{\partial h_2} & 0 & \cdots & 0 & 0 & 0 & 0 \\
\vdots & \vdots & \vdots & \vdots & \vdots & \vdots & \vdots & \vdots & \vdots & \vdots \\
0 & 0 & 0 & \frac{\partial C_i}{\partial Q_i} & \frac{\partial C_i}{\partial h_i} & \frac{\partial C_i}{\partial Q_{i+1}} & \frac{\partial C_i}{\partial Q_{i+1}} & 0 & 0 & 0 \\
0 & 0 & 0 & \frac{\partial M_i}{\partial Q_i} & \frac{\partial M_i}{\partial h_i} & \frac{\partial M_i}{\partial Q_{i+1}} & \frac{\partial M_i}{\partial Q_{i+1}} & 0 & 0 & 0 \\
\vdots & \vdots & \vdots & \vdots & \vdots & \vdots & \vdots & \vdots & \vdots & \vdots \\
0 & 0 & 0 & 0 & 0 & 0 & \frac{\partial C_{N-1}}{\partial Q_{N-1}} & \frac{\partial C_{N-1}}{\partial h_{N-1}} & \frac{\partial C_{N-1}}{\partial Q_N} & \frac{\partial C_{N-1}}{\partial h_N} \\
0 & 0 & 0 & 0 & 0 & 0 & \frac{\partial M_{N-1}}{\partial Q_{N-1}} & \frac{\partial M_{N-1}}{\partial h_{N-1}} & \frac{\partial M_{N-1}}{\partial Q_N} & \frac{\partial M_{N-1}}{\partial h_N} \\
0 & 0 & 0 & 0 & 0 & 0 & 0 & 0 & \frac{\partial DB}{\partial Q_N} & \frac{\partial DB}{\partial h_N}
\end{bmatrix}$$

The most difficult step when applying the Newton-Raphson algorithm is typically the evaluation of the partial derivative terms of the Jacobian matrix. For complex systems of equations, it can prove to be very difficult to determine analytically closed expressions for these partial derivatives. For this master's thesis, including the representative profiles for the momentum correction coefficient β, based on the output of the routine 'vul_sluis_impuls_straal_LVH.m', is the main reason why an analytical derivation of the partial derivatives is impeded. To that end, the Jacobian matrix is calculated numerically based on the definition of the partial derivative as

$$\frac{\partial f}{\partial x} = \frac{f(x+\varepsilon) - f(x)}{\varepsilon}$$

in the limit where ε becomes infinitely small. In a first attempt, the machine precision for MATLAB was implemented for ε[6]. However, this machine precision is variable, and depends on the number under consideration. This impedes the implementation in MATLAB, and leads to erroneous results (partial derivatives equal to zero when they are not). To that end, the parameter ε was hard-coded in 'Lock_Filling.m', and set equal to $10^{-8}$. The choice for this value follows from a comparison between the numerically and analytically determined Jacobian matrices for a steady state flow problem in a prismatic open channel (without including a momentum correction coefficient). Analytical expressions for the partial derivatives are derived for this situation.

With the Jacobian matrix $\vec{J}$ and the column vector $\vec{F}(\vec{x})$ determined, the system of equations

$$\vec{J} \cdot \delta\vec{x} = -\vec{F}(\vec{x})$$

is solved for the corrections $\delta\vec{x}$. This is done by applying a matrix solver such as Gaussian elimination, LU decomposition, etc. In the developped code 'Lock_Filling.m', the built-in MATLAB function 'mldivide' is applied. This function is especially efficient since the system of equations to be solved is analyzed first, after which 'mldivide' dispatches to an appropriate solver based on the lay-out and possible symmetry of the Jacobian matrix. In literature, the Thomas-Algorithm modified for block tridiagonal matrices, and the Fread algorithm, are typically mentioned as popular matrix solvers for the system of equations obtained by applying the Newton-Raphson algorithm to the 1D SWE. For this master's thesis these methods are not implemented.

The eventually obtained column vector $\delta\vec{x}$ contains the corrections on the current guess $\vec{x}$. The new guess $\vec{x}_{new}$ is obtained by applying the corrections to the current guess as

$$\vec{x}_{new} = \vec{x} + \delta\vec{x}$$

The iteration process is continued until a predetermined convergence level is achieved. The remark is made here that different convergence criteria are applied for the water level deviation h and the discharge Q as proposed in [15] as well as [16]. The tolerances for these corrections are hard-coded in 'Lock_Filling.m' and are equal to 1 mm for the water level deviation h, and 0.01 $m^3/s$ for the discharge Q. After each iteration, the maximum of the absolute values of the corrections for h and Q are determined, and compared to the specified tolerances.

As mentioned before, the convergence to the solution of the system of equations strongly depends on the initial guess for the unkown dependent variables. For the first time step, a good estimate is to use the initial conditions. For the following time steps, the solutions determined for the previous time step are used as initial guess.

[6] The machine precision of a number x in MATLAB can be determined by applying the built-in function 'eps(x)'.

# 6. Denderbelle Lock

An existing navigation lock is considered for studying the influence of the numerical solution method, and the influence of including representative profiles for the momentum correction coefficient β. For this master's thesis, this is the Denderbelle lock (river Dender, Flanders, Belgium).

Only numerical simulations for a lock chamber without a moored vessel are carried out[7]. Nevertheless, since both the flexible and rigid ship methods are implemented in the code 'Lock_Filling.m', the dimensions of the design ship for the Denderbelle lock are also described in this paragraph (Kristof Verelst, personal communication, July, 2017).

## 6.1. Lock Chamber

In Figure 12, the simplified geometry of the lock chamber for the Denderbelle lock is sketched, both in side and plan view.

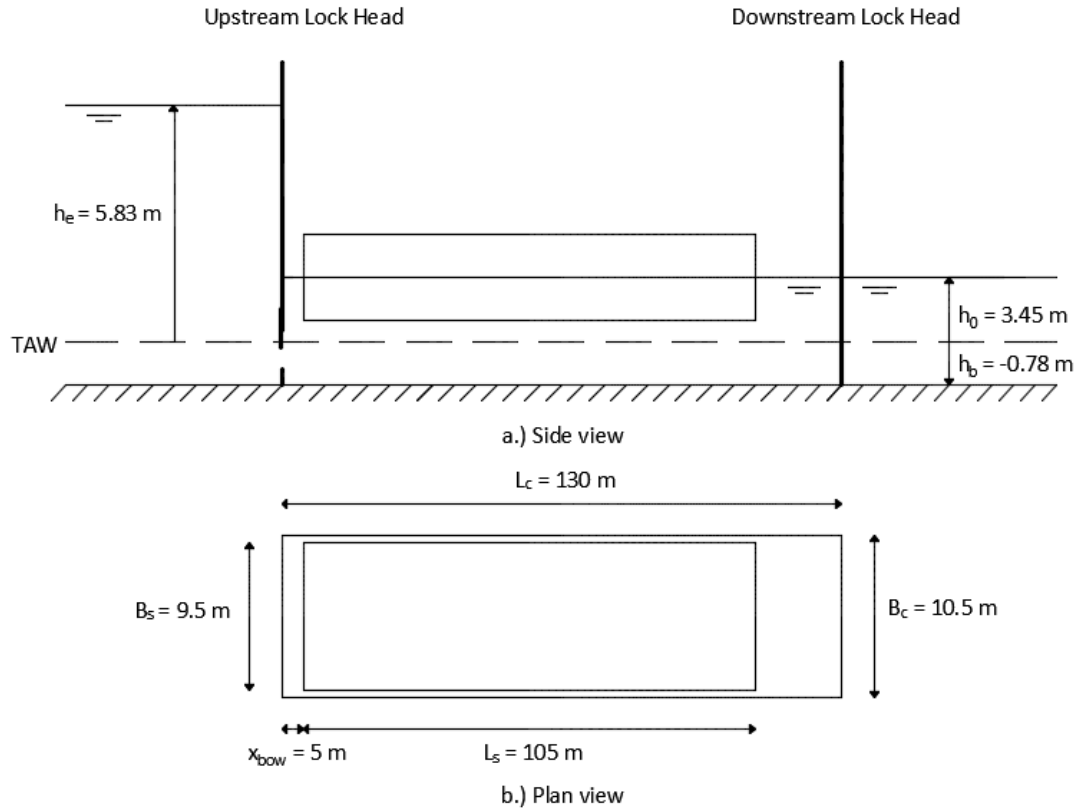


**Figure 12 – Simplified lock chamber geometry and design vessel dimensions for the Denderbelle lock**

[7] To that end, the flag 'i_ship' is specified to be equal to zero in 'Lock_Filling.m'.

The lock chamber has a length of 130 m and a width of 10.5 m. The initial water level in the lock chamber $h_0$, the equilibrium water level $h_e$ and the bottom level of the lock chamber $h_b$ are also summarized in Table 1. As mentioned before, the upper reach is assumed to be infinitely large for this master's thesis so that the water level of the upper reach is equal to the equilibrium water level $h_e$.

**Table 1 – Initial and equilibrium water levels and lock chamber bottom level**

| Parameter [Unit] | Value |
|---|---|
| $h_0$ [m TAW] | 3.45 |
| $h_e$ [m TAW] | 5.83 |
| $h_b$ [m TAW] | -0.78 |

The formula for the determination of the Chézy friction coefficient requires the specification of a roughness length $k_c$ for the lock chamber walls and bottom. This roughness length is assumed to be equal to 0.004 m, for both the lock chamber walls and bottom. This corresponds to the average value for the specified roughness length range for rough concrete in [9].

## 6.2. Design Vessel

For the Denderbelle lock, the design vessel is a CEMT class IV vessel. The dimensions of this design vessel, simplified to a rectangular box, are summarized in Table 2. This design vessel is also drawn in Figure 12.

**Table 2 – Dimension for the design vessel represented as a rectangular box**

| Parameter [Unit] | Value |
|---|---|
| $L_s$ [m] | 105.00 |
| $B_s$ [m] | 9.50 |
| $T_s$ [m] | 3.00 |

The distance between the bow of the moored vessel and the upstream lock gate is equal to 5 m. Typically a minimum distance of 5 m is proposed for the design of the lock chamber dimensions.

## 6.3. Boundary Conditions

For the determination of the filling discharge, both the head as a function of time (based on the equilibrium water level and the water level just downstream of the upstream lock gate), and the characteristics of the openings in the gate have to be specified. The required water levels are determined during the calculations, and the equilibrium water level is specified in paragraph 6.1. In this paragraph, the required input parameters to characterize the openings in the gates are described.

For the Denderbelle lock, the mitre gate contains six rectangular openings controlled by vertical lift valves. Each of these openings has a height of 0.9 metres and a width of 0.9 metres. In 'Lock_Filling.m',

the characteristics of each opening in the gates can be specified separately. However, since the openings are situated at the same level, and since their opening laws and discharge coefficient profiles are the same, the openings are modelled as one large opening with height 0.9 m and width 5.4 m. The top level of this gate opening is situated at 1.05 m above the TAW reference level.

Breaker logs are provided. However, the area of the filling jet just behind these breaker logs is specified to be equal to 4.86 $m^2$, which is equal to the total area of the gate openings. No spreading of the filling jet by the breaker logs is therefore assumed. The filling jet is assumed to enter the lock chamber horizontally.

The opening law for the vertical lift valves is described in Table 3.

**Table 3 – Opening law for the vertical lift valves**

| Time t [s] | Lift velocity $v_{lift}$ [m/s] |
|---|---|
| 0.00 | 0.0019 |
| 2000.00 | 0.0019 |

From Table 3 it is clear that the lift velocity of the vertical lift valves is constant in time. The lift height of the valve as a function of time is determined by integrating the profile for the lift velocity $v_{lift}$ as follows

$$h_{valve}(t) = \int_0^t v_{lift} dt = v_{lift} t + C = v_{lift} t$$

where the integration constant C is equal to zero since the lift height is assumed to be equal to zero at the start of the levelling process.

The relative lift height is obtained by dividing the above expression by the height of the gate openings

$$\theta(t) = \frac{h_{valve}(t)}{h_{valve}(t_{max})} = \frac{v_{lift} t}{h_{opening}}$$

where $t_{max}$ represents the time required to completely open the vertical lift valves so that the gate opening is completely opened. This time is determined as

$$t_{max} = \frac{h_{opening}}{v_{lift}} = \frac{0.9\ m}{0.0019\ \frac{m}{s}} = 473.68\ s$$

The relative lift height as a function of time is displayed in Figure 13.

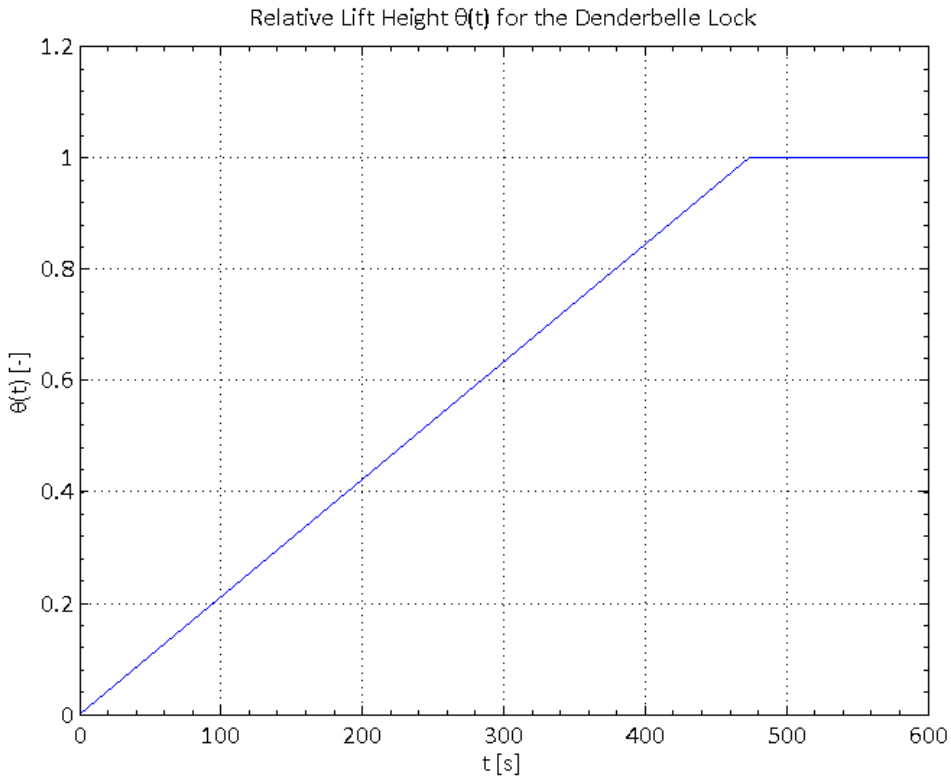


**Figure 13 – Relative lift height as a function of time for the Denderbelle lock**

Finally, the discharge coefficient as a function of the relative lift height is specified in Table 4.

**Table 4 – Discharge coefficient as a function of the relative lift height for the Denderbelle lock**

| Relative lift height θ(t) [-] | Discharge coefficient μ [-] |
|---|---|
| 0.00 | 0.95 |
| 0.15 | 0.82 |
| 0.28 | 0.78 |
| 0.40 | 0.75 |
| 1.00 | 0.75 |

This discharge coefficient as a function of the relative lift height is displayed in Figure 14.

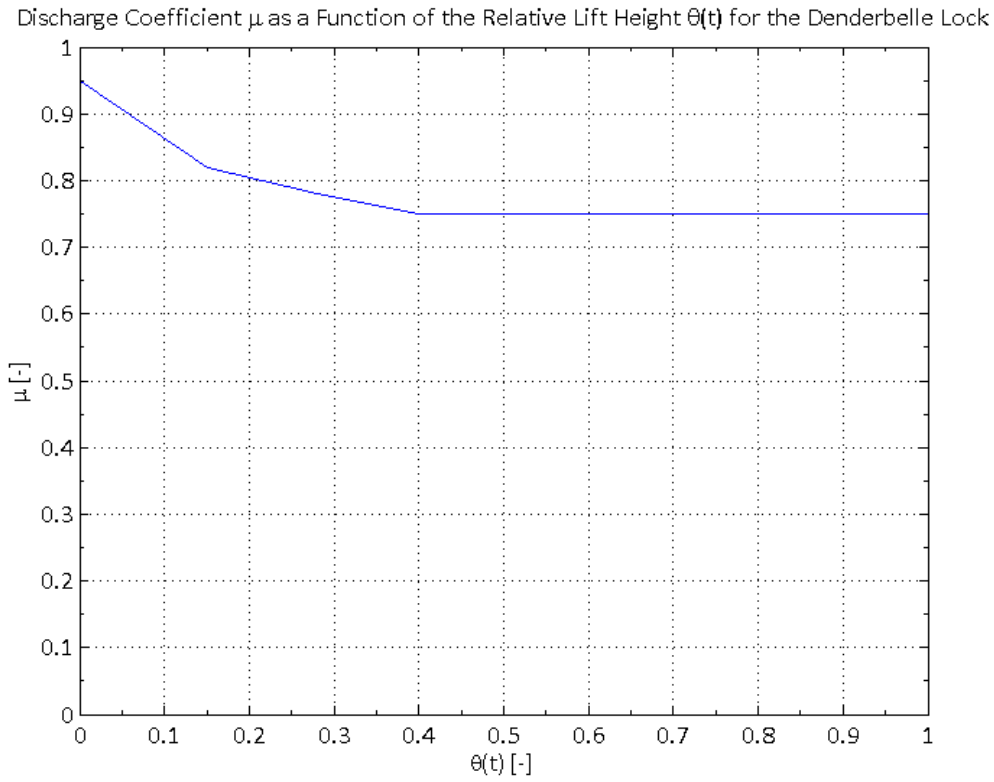


**Figure 14 – Discharge coefficient as a function of the relative lift height for the Denderbelle lock**

# 7. Description of the Filling Jet

For numerical codes such as LOCKFILL and 'vul_sluis.m', and codes solving the 1D SWE, the description of the filling jet still poses some challenges.

In this master's thesis, the function 'vul_sluis_impuls_straal_LVH.m' [17] is used for calculating representative values for the momentum correction coefficient as a function of the distance from the upstream lock gate after each time step. This function is based on relatively simple formulations for the determination of the discharge and the momentum for two-dimensional jets in finite water depths and in the presence of walls, as described in [18].

In the routine 'vul_sluis_impuls_straal_LVH.m', three main sections can be distinguished. In a first step, the length of the eddy above the filling jet is determined. Next, the discharge as a function of the distance from the jet origin is calculated. In a final step, the velocity profile and the momentum in the filling jet are calculated. For the exact expressions, and experimental results used for the validation of these expressions, the reader is referred to [17] and [18].

The momentum correction coefficient (sometimes referred to as the Boussinesq coefficient) is defined as [9]

$$\beta = \frac{\int_A \rho v^2 \, dA}{\rho U^2 A}$$

and represents the ratio of the momentum flux through a certain cross section for the real velocity profile, to the momentum flux through that cross section assuming a uniform velocity distribution, with magnitude equal to the cross sectional averaged velocity U.

Since the routine 'vul_sluis_impuls_straal_LVH.m' is based on formulations for two dimensional jets, and since the lock chamber is assumed to have a prismatic shape with a rectangular cross section, the following simplifications are carried out

$$\beta = \frac{B_c \int_0^{HK} \rho v^2 dh}{\rho U^2 B_c HK} = \frac{\int_0^{HK} v^2 dh}{U^2 HK}$$

The routine 'vul_sluis_impuls_straal_LVH.m' returns the discharge as a function of the distance from the upstream lock gate, as well as the integral of the squared velocities as required for the determination of the momentum correction coefficient β. The cross sectionally averaged velocity U is obtained by dividing the obtained discharges (in $m^2/s$) by the average water level in the lock chamber, indicated as HK in this routine. With these values, the momentum correction coefficient profile can be calculated for each time step.

It is noted here that two approaches can be selected for the determination of the velocity profile. The first approach mirrors the part of the velocity profile exceeding the water surface or lock chamber

bottom boundaries, about the applicable boundary. The second approach does not apply this mirroring.

The routine 'vul_sluis_impuls_straal_LVH.m' requires the following input arguments

| | |
|---|---|
| vs_versie | version number of the program 'vul_sluis' |
| QVO | discharge of the filling jet at the upstream lock gate |
| H_VS | height of the filling jet at the location of the upstream lock gate |
| H_VSm | height w.r.t. the lock chamber bottom of the midpoint of the filling jet (at the location of the upstream lock gate) |
| X | locations where the discharge and momentum of the filling jet are calculated |
| phi | angle of the filling jet with the horizontal (positive counterclockwise) |
| HK | water level in the lock chamber |

The parameters 'H_VS', 'H_VSm' and 'phi' follow from the characteristics of the gate openings as described in paragraph 6.3.

The discharge of the filling jet 'QVO' has to be specified in $m^2/s$. To that end, the filling discharge determined as described in paragraph 3.3, is divided by the width of the lock chamber. The width of the lock chamber is selected over the width of the gate openings because the one-dimensional approach followed in this master's thesis assures that the filling discharge applies to the complete cross section of the lock chamber immediately downstream of the upstream lock gate.

The formulae applied in the routine 'vul_sluis_impuls_straal_LVH.m' are actually only applicable to a filling jet entering a water volume at rest. During the levelling process, it is clear that the water volume in the lock chamber does not remain at rest and an assumption has to be made with respect to the input argument HK. For this master's thesis, HK is specified to be equal to the average water level in the lock chamber at each time step.

As a final remark, it is noted here that many assumptions are made for developping the routine 'vul_sluis_impuls_straal_LVH.m', as well as for applying this routine for the determination of representative profiles for the momentum correction coefficient β in this master's thesis.

# 8. Influence of the Numerical Solution Method

In this paragraph, the levelling process of the Denderbelle lock chamber without a moored vessel is simulated, without including momentum correction coefficient profiles based on the routine 'vul_sluis_impuls_straal_LVH.m'. For this reference case, the sensitivity of the obtained results to the numerical parameters is studied for the two implemented numerical solution methods. Based on this sensitivity analysis, adequate values for the numerical parameters are selected.

After having selected adequate values for the numerical parameters, the results obtained from both methods are compared, to study the influence of the adopted numerical solution method.

## 8.1. Sensitivity Analysis

When performing numerical simulations, smart choices have to be made for the numerical parameters specific to the applied numerical solution method. For the modified Stelling (1978) method, this means selecting a good combination of the spatial step Δx and time step Δt. For the Preissmann method, this means a good combination of the spatial step Δx, time step Δt, and the weighting factor θ. It is recommended to perform a sensitivity analysis on the obtained results when varying these numerical parameters.

The spatial step Δx typically follows from geometrical considerations. Even though a lock chamber without a moored vessel is modelled, the bow-to-stern slope will be calculated to approximate the longitudinal force as if a vessel is present in the lock chamber. Since the distance between the bow and the upstream lock gate is equal to 5 m, a spatial step of 2.5 m is selected both for the modified Stelling (1978) and the Preissmann method. This spatial step is not varied for this master's thesis.

### 8.1.1. Modified Stelling (1978)

For the modified Stelling (1978) method, the sensitivity of the results to variations of the time step Δt is studied. Since the modified Stelling (1978) method is an explicit method, the stability will be bound by some kind of CFL criterion as described in paragraph 4.3. The CFL number is calculated as

$$\sigma = \frac{c\Delta t}{\Delta x} = \frac{\sqrt{g(h_0 + h(x,t) - h_b)}\Delta t}{\Delta x}$$

where the characteristic velocity of the problem c is taken equal to the theoretical celerity for small surface waves in the absence of friction. By varying the time step Δt, it is clear that the CFL number will also vary for a fixed spatial step Δx. Since the water level deviation varies with respect to x and t, the CFL number will not be constant throughout the calculations and along the length of the lock chamber. Typically the CFL number is observed to lie within the range $[\sigma_0,\sigma_e]$ where the indices 0 and e indicate that respectively the initial water level and the equilibrium water level are used to calculate the CFL number.

The studied time steps for the modified Stelling (1978) method are summarized in Table 5, together with a representative range for the CFL number.

**Table 5 – Studied time steps for the modified Stelling (1978) method**

| Simulation # | Δt [s] | $\sigma_0$ [-] | $\sigma_e$ [-] |
|---|---|---|---|
| 1 | 0.01 | 0.026 | 0.032 |
| 2 | 0.10 | 0.258 | 0.322 |
| 3 | 0.20 | 0.515 | 0.644 |
| 4 | 0.30 | 0.773 | 0.966 |
| 5 | 0.40 | 1.031 | 1.288 |
| 6 | 0.85 | 2.190 | 2.738 |
| 7 | 0.90 | 2.319 | 2.899 |

The time steps were selected as to gradually vary the CFL number from very small values up to values in the neighbourhood of one. To illustrate the stability behaviour of the modified Stelling (1978) method, the last two simulations were added afterwards. For a time step equal to 0.85 s, the maximum CFL number is still smaller than the limit for stability on the imaginary axis displayed in Figure 8 (equal to $2\sqrt{2}$). For a time step of 0.90 s the maximum CFL number becomes higher than the described limit, and the results become unstable (negative water levels in the lock chamber).

In Figure 15, the filling discharge (dimensionless with respect to the maximum filling discharge) is displayed as a function of time (dimensionless with respect to the levelling time $t_{niv,2}$). The levelling time $t_{niv,2}$ denotes the first instant in time where the absolute value of the difference between the equilibrium water level and the average water level in the lock chamber is smaller than 1 mm.

A first observation with respect to Figure 15, is that varying the time step Δt does not significantly influence the results before $t_{niv,2}$. The general profile of the filling discharge curve corresponds to the expected curve for filling through openings in the gates with a constant lift velocity for the vertical lift valves, yet a variable discharge coefficient.

After $t_{niv,2}$, the discharge is expected to go to zero. For the first two simulations (Δt = 0.01 s and Δt = 0.10 s), the filling discharge displays an oscillating behaviour towards zero. For the other simulations, the filling discharge is observed to behave irregularly and approaches constant values differing from zero. The absolute value of this erroneous constant value for long simulation times increases when the time step is increased.

A first hypothesis proposed to resolve these unexpected results for longer simulation times, deals with the calculation of the filling discharge boundary condition. As described in paragraph 3.3, the head as a function of time, for the calculation of the filling discharge, is calculated as the difference between the equilibrium water level $h_e$ and the water level just downstream of the upstream lock gate. Due to the space staggered grid, the water level just downstream of the lock gate has to be determined by linear extrapolation. In LOCKFILL and 'vul_sluis.m', the head as a function of time is determined based

on the average water level in the lock chamber at each time step. This approach is also implemented in 'Lock_Filling.m' to verify whether this leads to better results for longer simulation times. The obtained results are described in Appendix D. For longer calculation times, the discharge is still observed to oscillate around zero, and these oscillations are even observed to increase for longer calculation times. The calculation of the filling discharge boundary condition, does not explain the observations after $t_{niv,2}$ for the higher time steps.

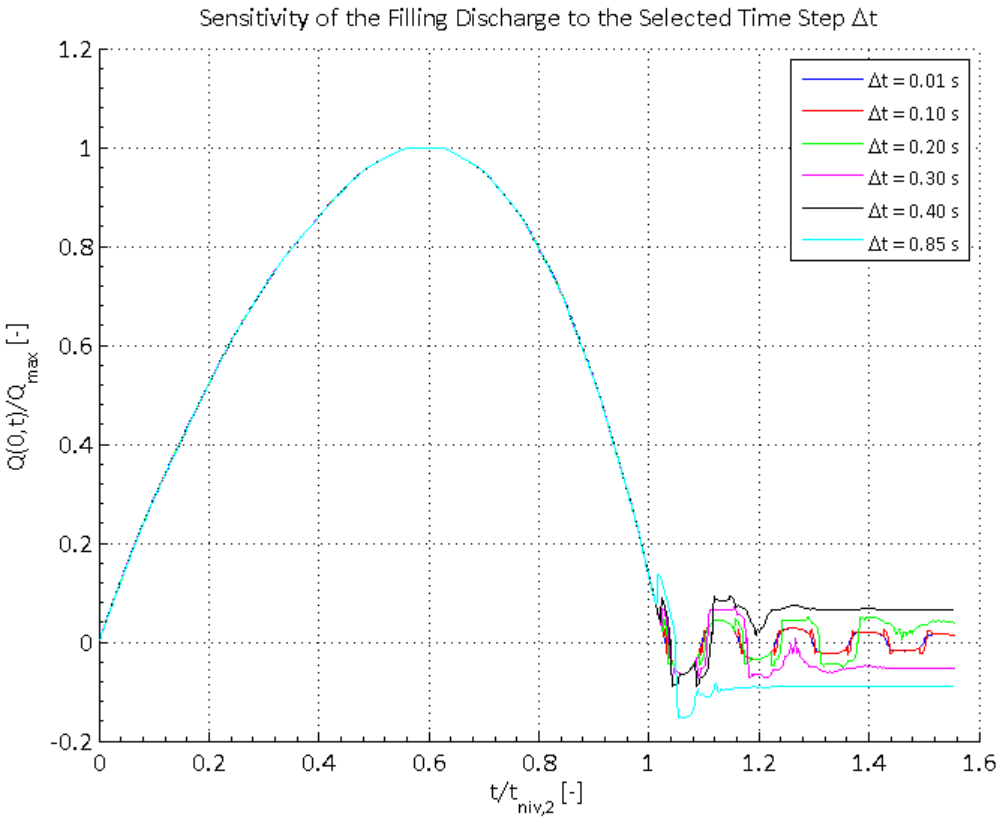


**Figure 15 – Sensitivity of the filling discharge to the time step Δt for the modified Stelling (1978) method**

In Figure 16, the head (dimensionless with respect to the initial head $h_e$-$h_0$) is displayed as a function of time (dimensionless with respect to the filling time $t_{niv,2}$). No significant differences in the results are observed for the different studied time steps Δt. Except for simulations one and two, the head is observed to approach a small residual value differing from zero for longer calculation times (not clearly visible in Figure 16 without zooming in).

Figure 17 displays the bow-to-stern slope as a function of time. This slope of the water surface between the bow and the stern of a moored vessel, is often used to approximate the longitudinal force on the moored vessel. Even though a lock chamber without a moored vessel is studied, the bow-to-stern slope is studied due to its importance for the estimation of the longitudinal forces on a vessel. The variation of the bow-to-stern slope in time is observed to correspond well with the variation of the longitudinal force component due to translatory waves. The bow-to-stern slope is observed to display an oscillating

behaviour, with mainly positive values before the maximum filling discharge is reached, and mainly negative values afterwards.

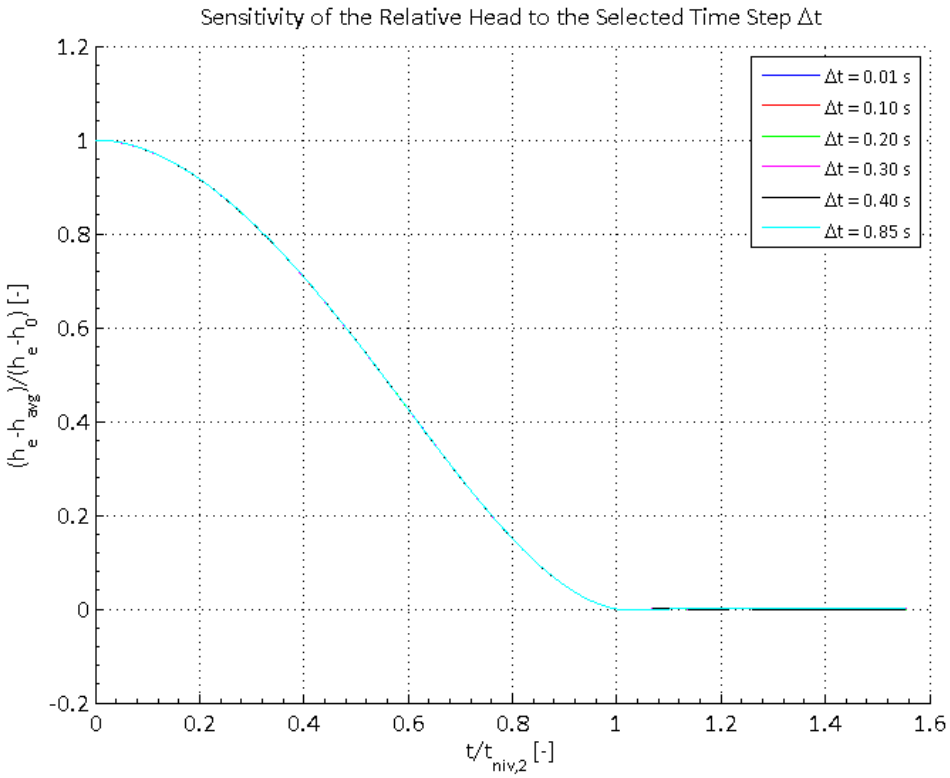


**Figure 16 – Sensitivity of the relative head to the time step Δt for the modified Stelling (1978) method**

As for the filling discharge and the head, the bow-to-stern slope is expected to go to zero after $t_{niv,2}$. However, the bow-to-stern slope is observed to slowly oscillate towards zero for simulations one and two, yet displays more irregular behaviour after $t_{niv,2}$ for simulations three to six, and this behaviour becomes more pronounced for higher values of the time step Δt.

In [7], G.S. Stelling notes that when the lock chamber is completely or almost completely filled, the hawser forces are observed to strongly oscillate, without the calculated results becoming unstable. By chosing a small enough time step Δt, the problem was resolved. A possible explanation for these oscillations is proposed. At the end of the levelling process, the partial derivatives occuring in the 1D SWE approach zero. Since the applied numerical scheme does not contain a lot of numerical damping, small perturbations caused by truncation errors become more important, leading to the observed oscillations.

As in [7] it is noted that in fact, the end of the levelling process is of lesser importance since in practice the lock gates would already have been opened in this phase of the numerical simulation. Nevertheless the observed oscillations should not be the consequence of programming mistakes. To that end, the numerically obtained results with the modified Stelling (1978) method are compared to the obtained results with the Preissmann scheme in paragraph 8.2.

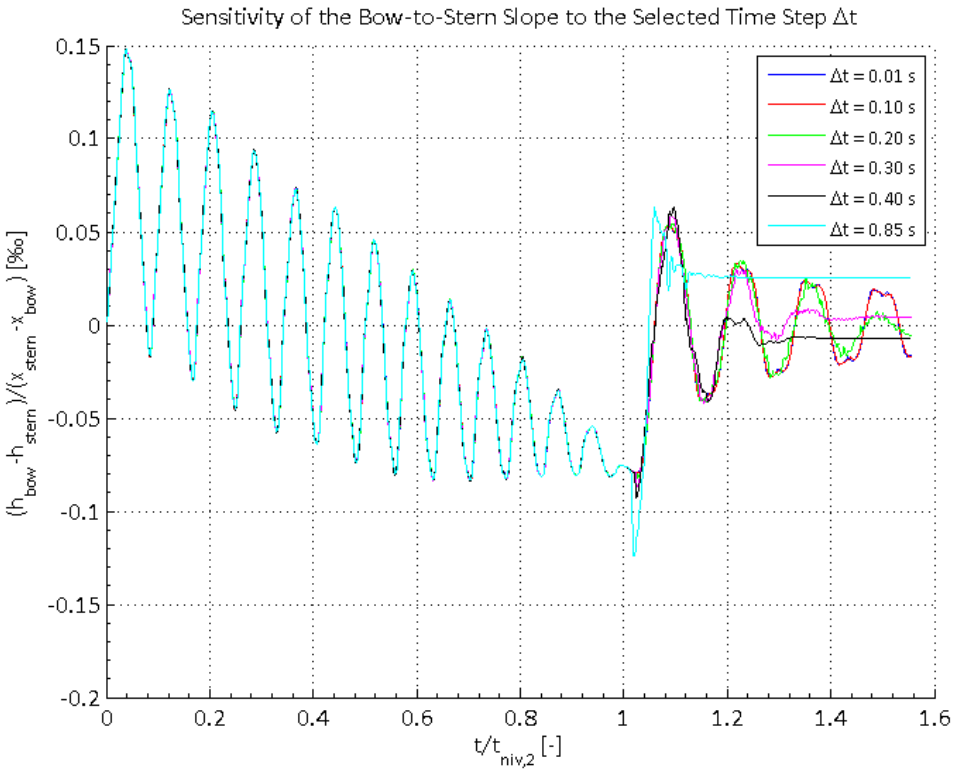


**Figure 17 – Sensitivity of the bow-to-stern slope to the time step Δt for the modified Stelling (1978) method**

To conclude, no well-grounded explanation for the observed behaviour of the filling discharge, the head and the bow-to-stern slope for longer simulation times is found. As described by G.S. Stelling [7], chosing a sufficiently small time step seems to resolve the problem. To that end, the smallest time step Δt equal to 0.01 s is selected for the modified Stelling (1978) method, in combination with the proposed spatial step Δx of 2.5 m.

### 8.1.2. Preissmann

For the Preissmann method, the sensitivity of the results to variations of the time step Δt and the weighting factor θ is studied. The studied time steps for the Preissmann method are summarized in Table 6, along with the applicable range of CFL numbers determined as described in paragraph 8.1.1.

**Table 6 – Studied time steps for the Preissmann method**

| Simulation # | Δt [s] | $\sigma_0$ [-] | $\sigma_e$ [-] |
|---|---|---|---|
| 1 | 0.25 | 0.64 | 0.81 |
| 2 | 0.40 | 1.03 | 1.29 |
| 3 | 0.50 | 1.29 | 1.61 |
| 4 | 1.00 | 2.58 | 3.22 |
| 5 | 2.00 | 5.15 | 6.44 |
| 6 | 4.00 | 10.31 | 12.88 |

The studied time steps are selected in such a manner as to study different ranges for the CFL number. To that end, CFL values smaller than one, larger than one but close to one, and larger than one are studied. Based on the graphs for the numerical damping and dispersion displayed in paragraph 5.2, the numerical damping and dispersion are expected to increase when the time step Δt is increased (for a constant spatial step Δx).

The obtained results for the filling discharge, the head, and the bow-to-stern slope as a function of time are respectively displayed in Figure 18, Figure 19, and Figure 20. The studied parameters are made dimensionless in the same manner as in the previous paragraph.

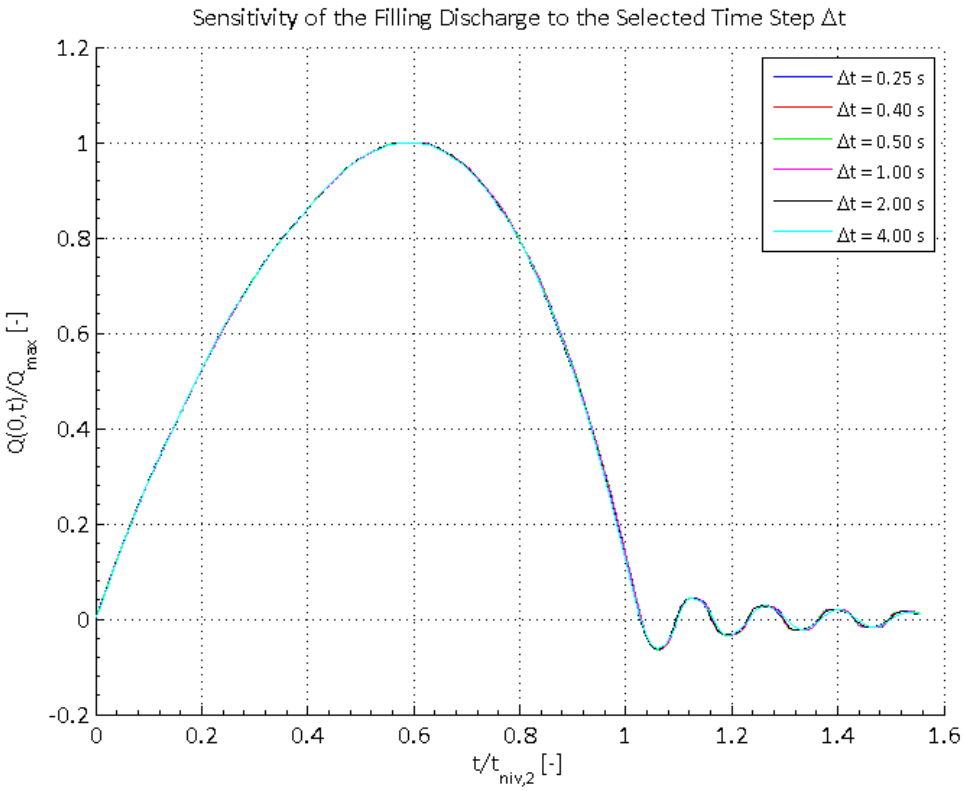


**Figure 18 – Sensitivity of the filling discharge to the time step Δt for the Preissmann method**

From Figure 18 and Figure 19, it is clear that increasing the time step Δt does not lead to significant differences in the results for the filling discharge and the head as a function of time. Furthermore, it is noted that the behaviour of the filling discharge and the head for longer simulation times (after $t_{niv,2}$), better corresponds with the expectations. The filling discharge and the head oscillate towards zero after $t_{niv,2}$. It is repeated here that also for the Preissmann method, the filling discharge is calculated based on the head determined from the difference between the equilibrium water level $h_e$ and the water level just downstream of the upstream lock gate. However, no linear extrapolation is required to determine this water level due to the applied collocated grid.

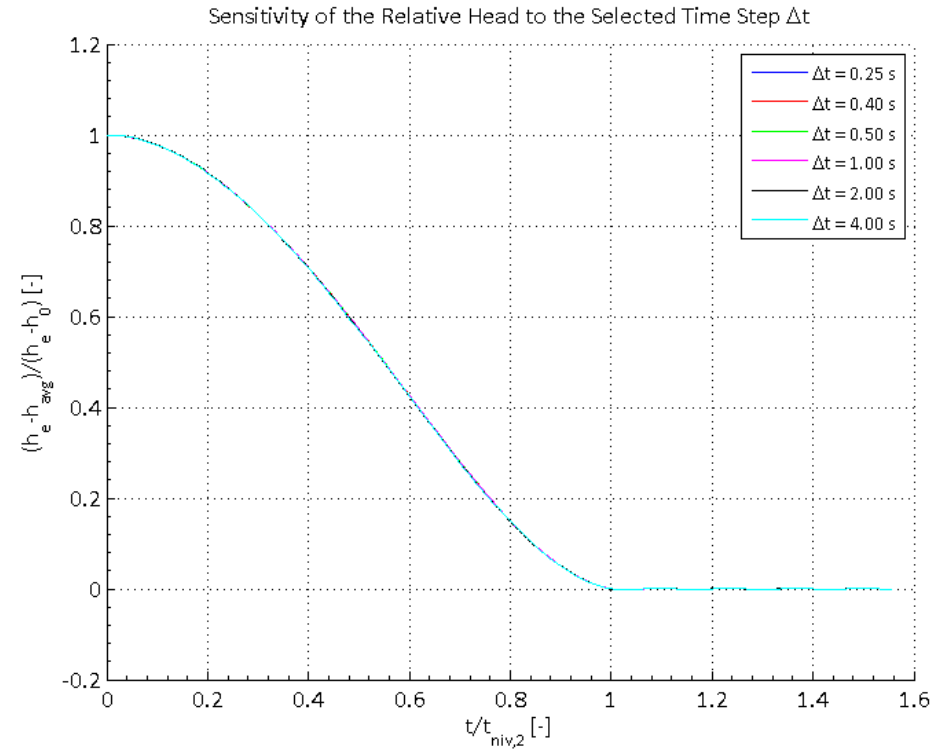


**Figure 19 – Sensitivity of the relative head to the time step Δt for the Preissmann method**

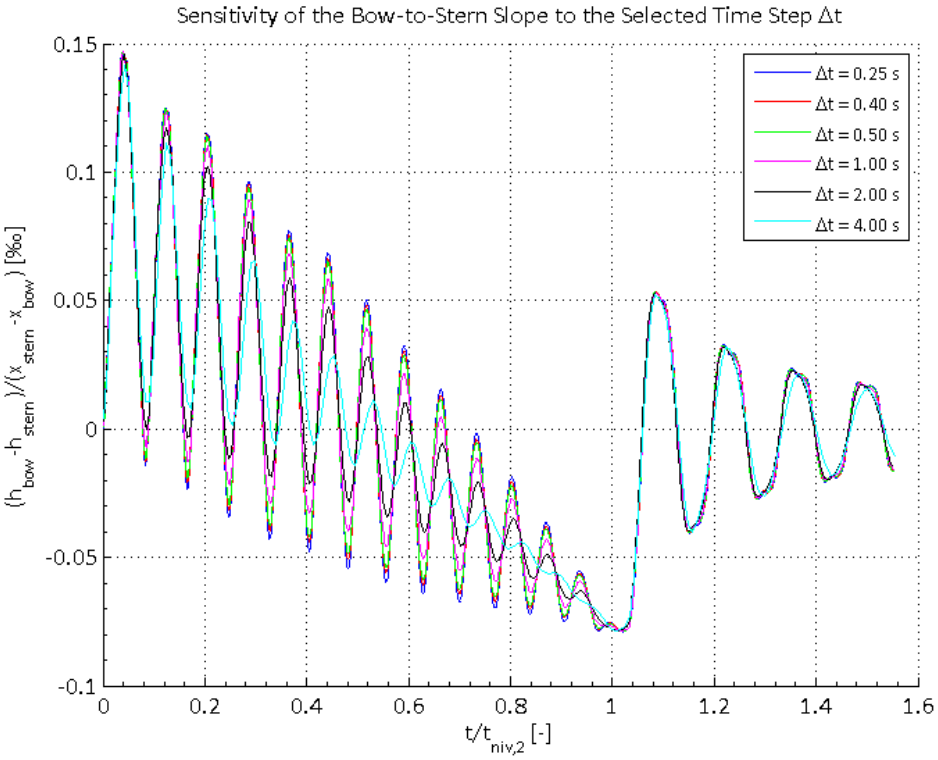


**Figure 20 – Sensitivity of the bow-to-stern slope to the time step Δt for the Preissmann method**

From Figure 20, the increased numerical damping can be clearly observed for increasing the time step Δt. After $t_{niv,2}$, the obtained results correspond with each other, and oscillate towards zero. The time step Δt equal to 0.50 s is selected since the results for the bow-to-stern slope correspond well for the first three simulations. For higher time steps, the numerical damping becomes more and more pronounced.

For this selected time step, the influence of the weighting factor θ of the Preissmann method on the numerical results is studied. In [6], it is remarked that for reasons of accuracy, the parameter θ should be selected close to 0.5. However values to close to 0.5 can result in solutions with undesirable numerical oscillations. Increasing the value for the parameter θ above 0.5 increases numerical damping, and as such eliminates numerical oscillations, yet at the expense of reduced accuracy. Typically the parameter θ is therefore selected in the range of 0.55 to 0.70.

The parameter θ is varied in the range of 0.55 to 0.70 to verify the influence on the numerical results. For the filling discharge and the head as a function of time, no noticeable differences are observed, and these graphs are therefore not repeated. The bow-to-stern slope as a function of time is displayed in Figure 21 for different values for the parameter θ. The increased numerical damping when the parameter θ is increased (away from 0.5) is clearly observed.

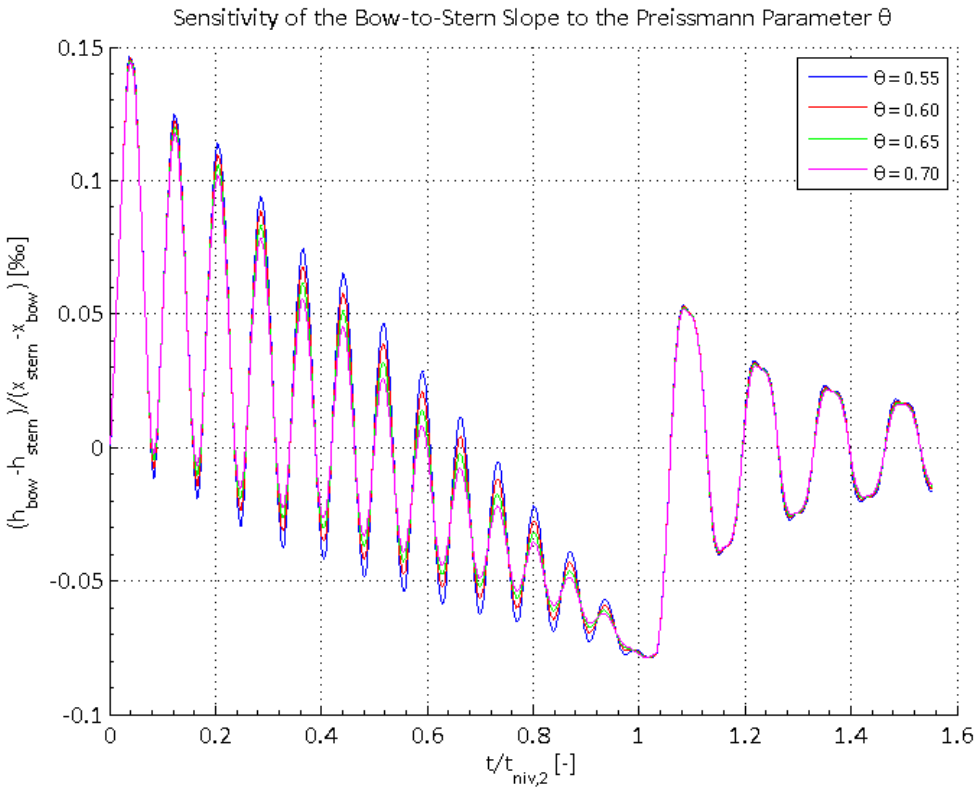


**Figure 21 – Sensitivity of the bow-to-stern slope to the parameter θ for the Preissmann method**

For this master's thesis the parameter θ of the Preissmann scheme is set equal to 0.55, which is the default value in LOCKSIM [6].

## 8.2. Comparing Modified Stelling (1978) to Preissmann

Now that adequate values for the numerical parameters have been selected, the influence of the numerical solution method on the obtained results is studied. To provide a clear overview, the selected numerical parameters for both methods are summarized in Table 7.

**Table 7 – Selected numerical parameters for the modified Stelling (1978) and the Preissmann method**

| Parameter [Unit] | Modified Stelling (1978) | Preissmann |
|---|---|---|
| Δx [m] | 2.50 | 2.50 |
| Δt [s] | 0.01 | 0.50 |
| θ [-] | N/A | 0.55 |

In Figure 22, Figure 23 and Figure 24, the filling discharge, the head and the bow-to-stern slope are respectively displayed as a function of time, for both the modified Stelling (1978) and the Preissmann method. These graphs are made dimensionless in the same manner as before.

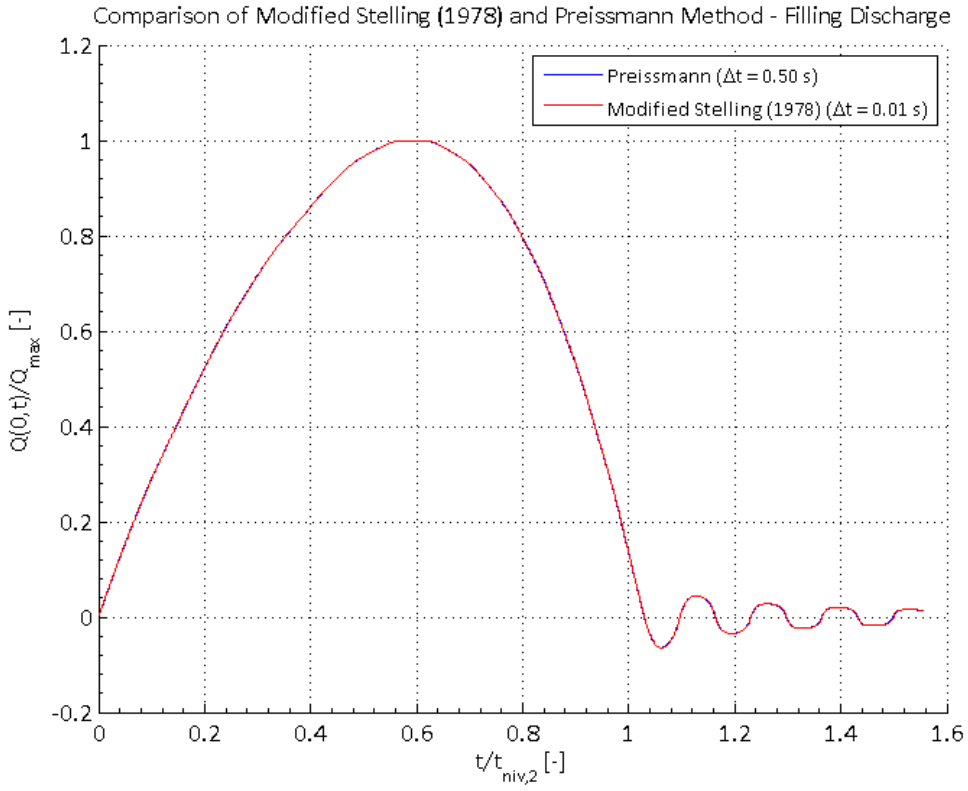


**Figure 22 – Filling discharge as a function of time for both the modified Stelling (1978) and the Preissmann method**

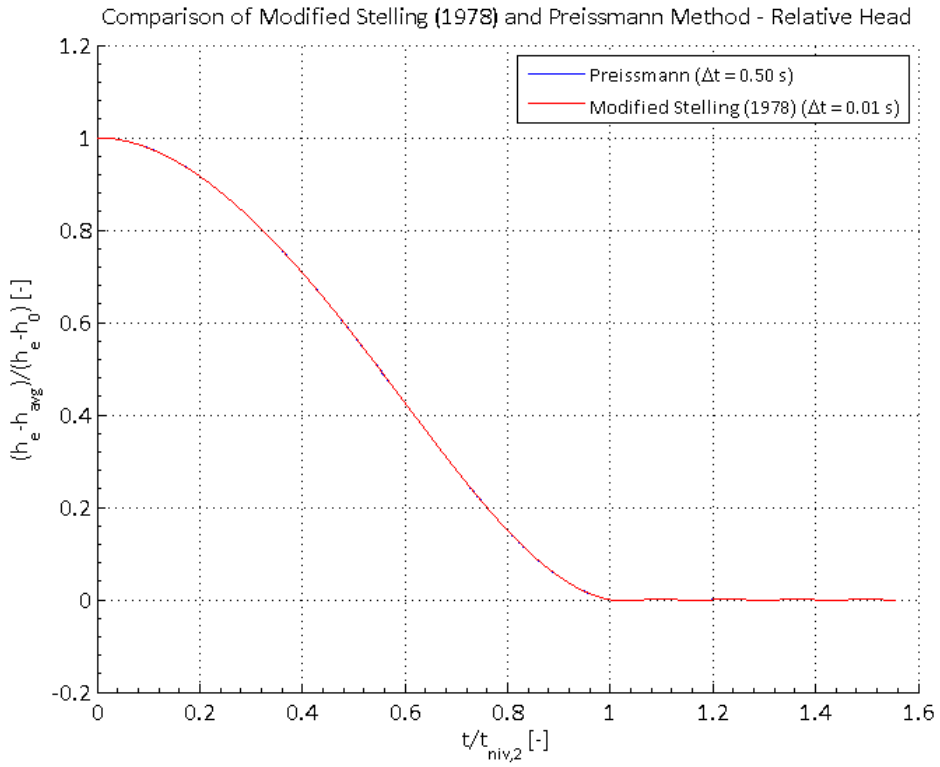


**Figure 23 – Relative head as a function of time for both the modified Stelling (1978) and the Preissmann method**

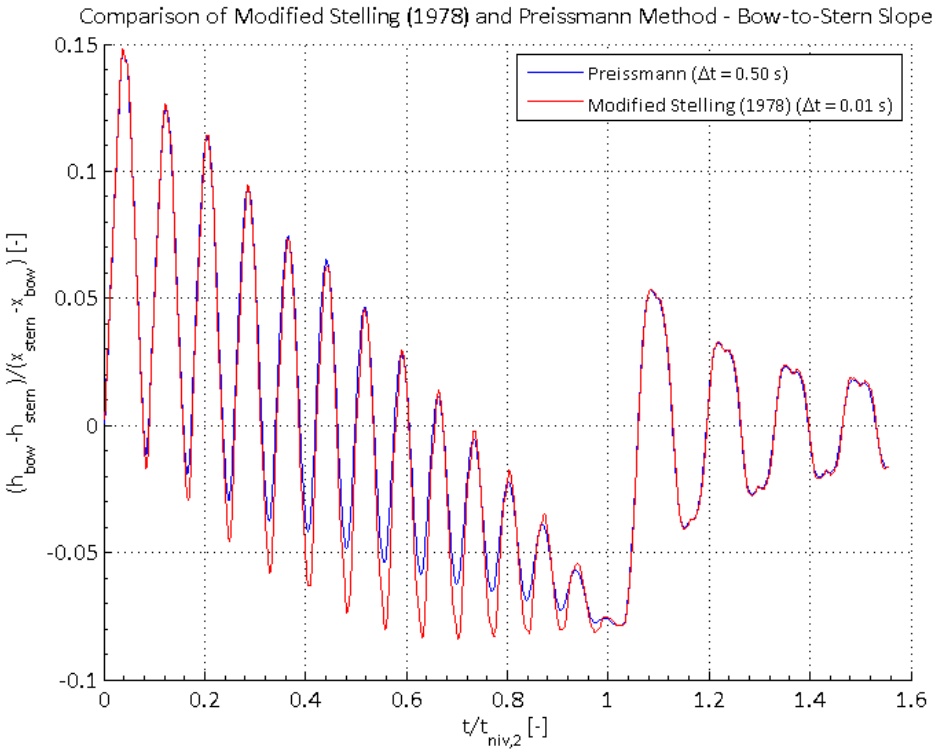


**Figure 24 – Bow-to-stern slope as a function of time for both the modified Stelling (1978) and the Preissmann method**

No significant differences are observed between the results for the filling discharge and the head as a function of time (Figure 22 respectively Figure 23).

For the bow-to-stern slope (Figure 24), differences are observed before $t_{niv,2}$. The values for the bottom peaks are quite a bit lower for the modified Stelling (1978) method compared to the Preissmann method. The top peaks correspond better with each other. After $t_{niv,2}$, no remarkable differences are observed and the bow-to-stern slope oscillates towards zero for both methods.

Finally, a remark is made with respect to the required calculation time for both methods[8]. For the selected numerical parameters, the calculation times for the modified Stelling (1978) and Preissmann methods are respectively equal to 96 seconds and 42.88 minutes. By only considering the required calculation time, the modified Stelling (1978) method is clearly preferable over the Preissmann method. The large difference in the required calculation time is mainly attributed to the fact that for the Preissmann method, a system of non-linear equations has to be solved iteratively for each time step.

[8] The calculation time is determined by using the 'Run and Time' option in MATLAB.

# 9. Influence of the Momentum Correction Coefficient β

In this final paragraph the influence of including representative profiles for the momentum correction coefficient β is studied. The momentum correction coefficient is included in order to better represent a two-dimensional filling jet in this one-dimensional model.

For each time step, the output of the function 'vul_sluis_impuls_straal_LVH.m' is used to determine representative profiles for the momentum correction coefficient as a function of the distance from the upstream lock gate, as described in paragraph 7.

For the Preissmann method, the required calculation time is of the order of weeks when including profiles for the momentum correction coefficient. To be able to apply the Preissmann method when including the momentum correction coefficient, the developped code still has to be optimized. The long calculation times are the result of the many calls of the routine 'vul_sluis_impuls_straal_LVH.m'. Including the momentum correction coefficient when applying the modified Stelling (1978) method also leads to a tremendous increase in the required calculation time.

In the following, the influence of including the momentum correction coefficient is only studied for the modified Stelling (1978) method and for the in paragraph 8.1.1 selected numerical parameters. First a typical profile for the momentum correction coefficient as a function of the distance from the upstream lock gate is discussed.

## 9.1. Typical Momentum Correction Coefficient Profile

To gain some more insight with respect to the applied profiles for the momentum correction coefficient β, a typical profile is displayed in Figure 25. This profile applies to the instant in time when the maximum filling discharge $Q_{max}$ is reached.

By studying Figure 25, it is noted that the largest values for the momentum correction coefficient β occur just downstream of the upstream lock gate through which filling takes place. The momentum correction coefficient decreases to a value of one when moving further away from the upstream lock gate. This minimum value is enforced by a line of code stating that the momentum correction coefficient can not become lower than one.

The distance between the upstream lock gate and the first cross section where the momentum correction coefficient becomes equal to one, is indicated as the influence length of the momentum correction coefficient. This influence length is a function of time, and increases from a value of about 0.20 times $L_c$ to a value of about 0.40 $L_c$. The influence length is clearly larger than the distance between the bow and the upstream lock gate (as specified in paragraph 6.2). This further justifies studying the influence of including the momentum correction coefficient β for the estimation of the longitudinal forces on a moored vessel.

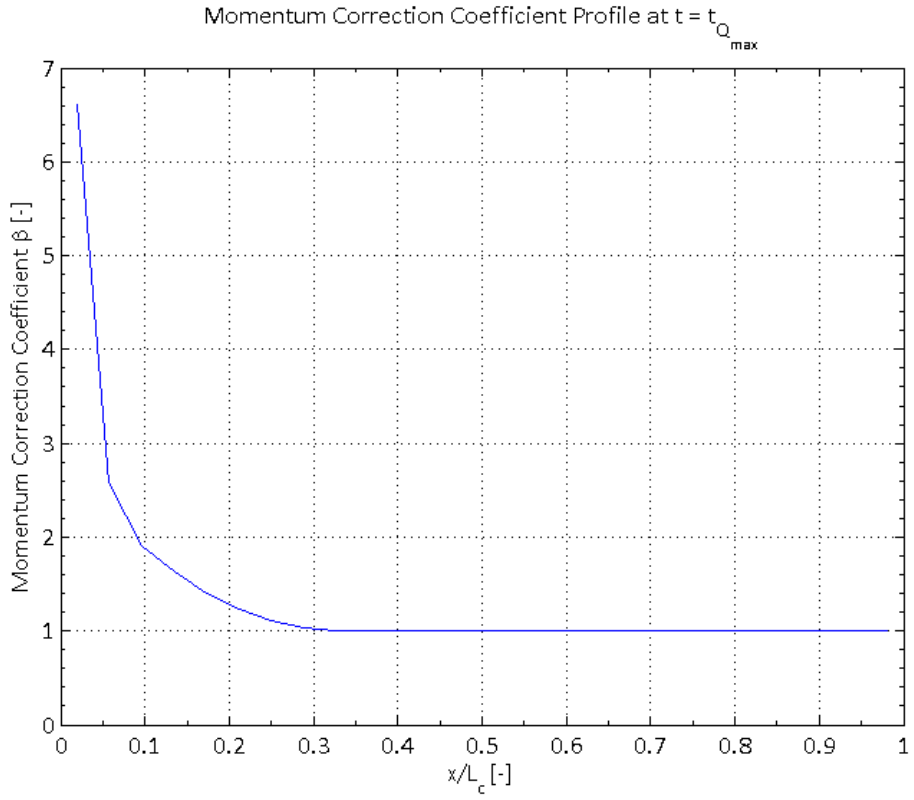


**Figure 25 – Typical profile for the momentum correction coefficient as a function of the distance from the upstream gate**

The peak values of the momentum correction coefficient (just downstream of the upstream lock gate) increase from about 5.75 at the beginning of the levelling process to a maximum value of about 6.95 and then decrease again to a value of about 5.60 at the end of the levelling process.

## 9.2. Comparison for the Filling Discharge, Head and Bow-to-Stern Slope

In Figure 26, Figure 27 and Figure 28, the filling discharge, the head and the bow-to-stern slope are displayed as a function of time for the modified Stelling (1978) method, with and without including representative profiles for the momentum correction coefficient. The displayed parameters are made dimensionless in the same manner as in the previous paragraphs. The case where no momentum correction coefficient is included is indicated with the label 'β = 1.0'. The case where the momentum coefficient is included based on the output of the routine 'vul_sluis_impuls_straal_LVH.m' is indicated with the label 'β = f(x,t)'.

From Figure 26 and Figure 27 it is observed that including representative profiles for the momentum correction coefficient does not lead to significant differences in the results for the filling discharge and the head as a function of time.

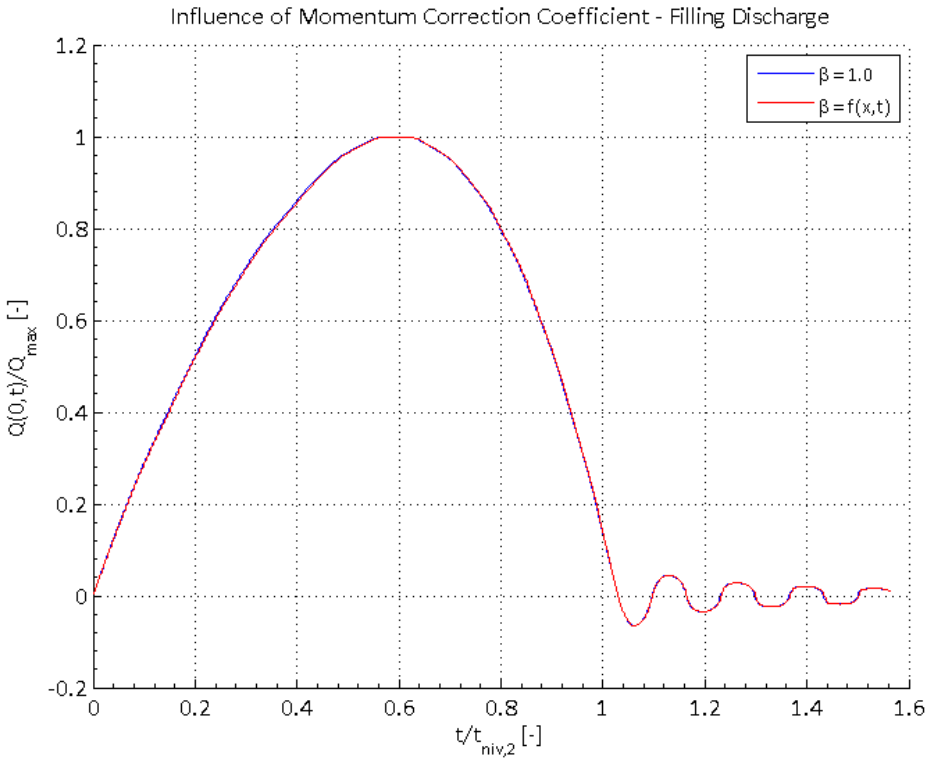


**Figure 26 – Influence of the momentum correction coefficient on the filling discharge**

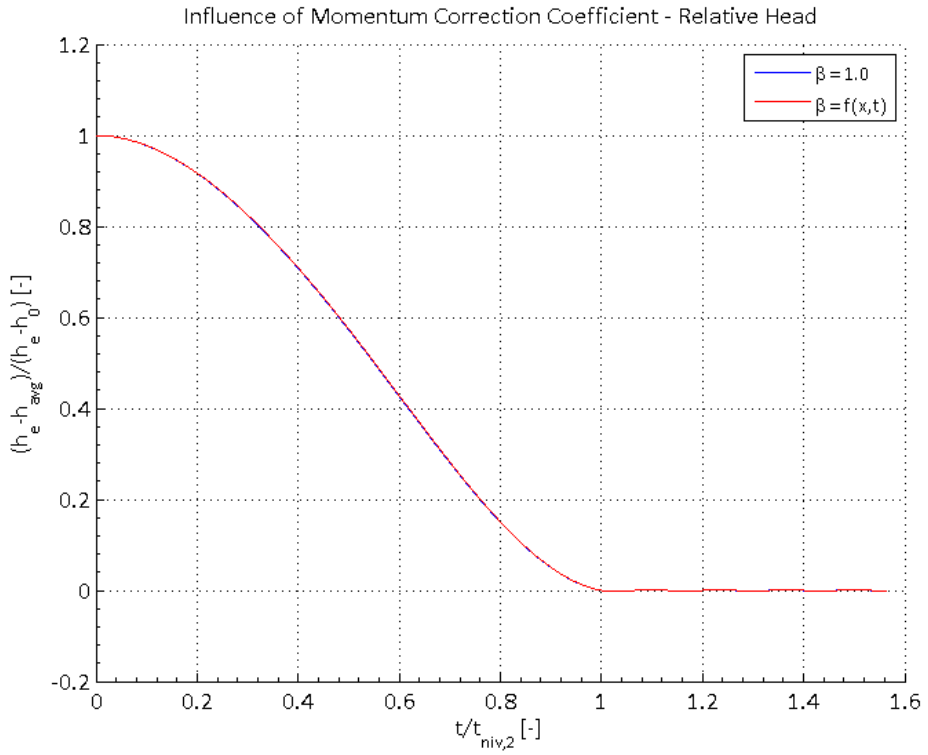


**Figure 27 – Influence of the momentum correction coefficient on the relative head**

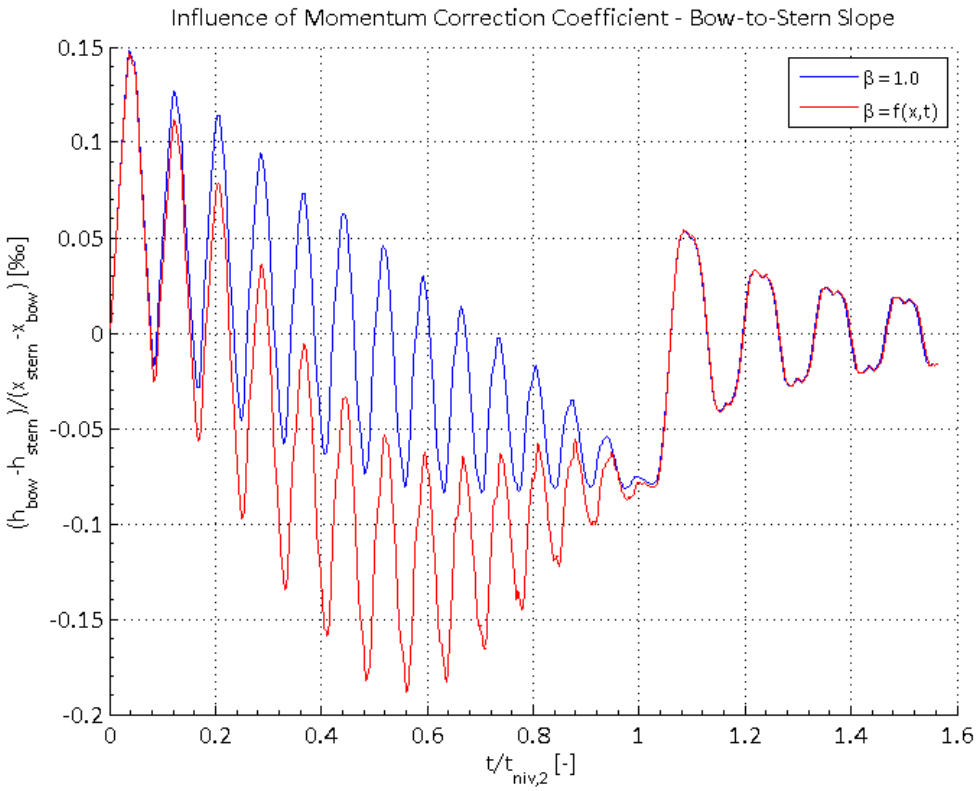


**Figure 28 – Influence of the momentum correction coefficient on the bow-to-stern slope**

However, for the bow-to-stern slope displayed in Figure 28, significant differences are observed when the momentum correction coefficient is included in the calculations. With the momentum correction coefficient equal to one, the variation of the bow-to-stern slope corresponds to the typical variation of the longitudinal force component due to translatory wave effects as described before. By including the momentum correction coefficient profiles based on the routine 'vul_sluis_impuls_straal.m', the oscillatory behaviour attributed to the translatory wave effect is still observed, but the overall curve displays a downwards deflection. This variation of the bow-to-stern slope corresponds to the variation of the longitudinal force component due to both the translatory wave and the momentum decrease effects.

As described in paragraph 2, LOCKFILL determines the contribution of the momentum decrease to the longitudinal force on the vessel based on the combination of two effects. Both the decrease of the discharge in the longitudinal direction (away from the upstream lock gate), and the decrease of the high flow velocities in the longitudinal direction (due to the concentrated filling jet), cause a total decrease of the momentum along the length of the vessel.

The decrease of the discharge in the longitudinal direction is automatically described by applying the 1D SWE (even when the momentum correction coefficient is not included). This decrease of the discharge in the longitudinal direction is displayed in Figure 29 for the instant in time where the maximum filling discharge is reached. Some differences are observed when including the momentum

correction coefficient profiles based on 'vul_sluis_impuls_straal_LVH.m', but the approximately linear decrease of the discharge away from the upstream lock gate is still observed.

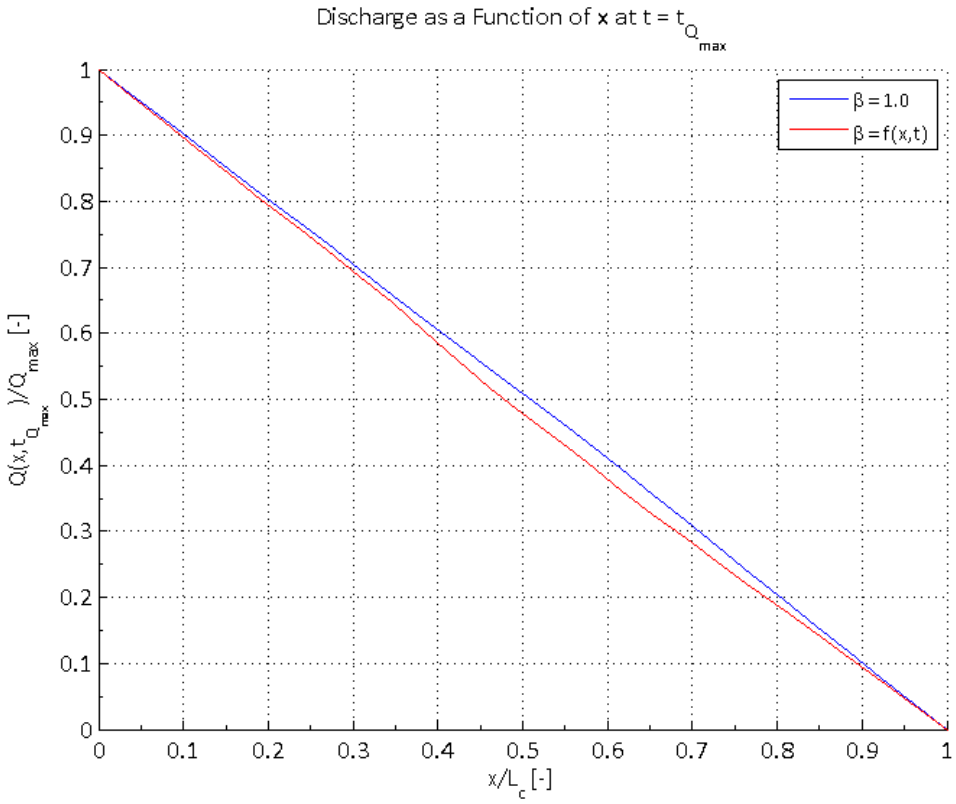


**Figure 29 – Linear decrease of the discharge away from the upstream lock gate (at t = $t_{Qmax}$)**

For the case where the momentum correction coefficient is equal to one, the two-dimensional filling jet is not represented, and therefore the decrease of the high flow velocities due to the concentrated filling jet are certainly not represented. By including the momentum correction coefficient based on the routine 'vul_sluis_impuls_straal_LVH.m', the filling jet is represented within β, so that the decrease of the high flow velocities due to the filling jet are also represented.

Based on these observations, and the influence of including the momentum correction coefficient on the bow-to-stern slope as observed in Figure 28, it is assumed that the water level differences between the bow and the stern of the vessel account for both the translatory wave and the momentum decrease effects, which are considered separately in LOCKFILL [4] and 'vul_sluis.m' [5].

Further research is therefore recommended with respect to the determination of the longitudinal force component due to the momentum decrease effect in LOCKFILL and 'vul_sluis.m', in order to determine whether these effects are inherently included in a 1D SWE model, by applying appropriate profiles for the momentum correction coefficient β.

# 10. Conclusion

In 'Lock_Filling.m' both the modified Stelling (1978) method and the Preissmann method are implemented for the solution of the 1D SWE to model the water movement in a lock chamber during filling and emptying. The presence of a moored vessel is also implemented for both the flexible and the rigid ship approaches, but is not further considered in this master's thesis. With respect to the development of the code 'Lock_Filling.m', it is noted that a lot of time was consumed to debug and optimize the written code.

The Denderbelle lock is then considered to study the obtained results for filling the lock chamber without a moored vessel.

First, the importance of selecting adequate values for the numerical parameters for the two implemented numerical solution methods is emphasized. To that end, a sensitivity analysis is performed for the time step $\Delta t$ of the modified Stelling (1978) method, and for the time step $\Delta t$ and the weighting factor $\theta$ of the Preissmann method. In order to avoid undesirable effects for longer calculation times, a very small time step is selected for the modified Stelling (1978) method. To avoid excessive numerical damping and dispersion, the parameter $\theta$ for the Preissmann method is set equal to 0.55 and a time step is selected in order to obtain CFL numbers larger than, but close to one.

No significant differences are observed when comparing the results for the time evolution of the filling discharge and the head between the results obtained with the modified Stelling (1978) method and the Preissmann method. For the bow-to-stern slope, some differences are observed between the results obtained with the modified Stelling (1978) and the Preissmann method. The downward peaks are observed to be lower for the former method.

For studying the influence of including representative profiles for the momentum correction coefficient based on the output of the routine 'vul_sluis_impuls_straal_LVH.m', the Preissmann method is not further considered due to the disproportionately long calculation times. For the modified Stelling (1978) method, it is noted that the calculation times are also observed to increase significantly.

For the time evolution of the filling discharge and the head, including representative profiles for the momentum correction coefficient does not lead to significant differences in the results. For the time evolution of the bow-to-stern slope, important differences are observed. Without including the momentum correction coefficient, the variation of the bow-to-stern slope is observed to correspond with the variation of the longitudinal force due to the translatory wave effect (oscillatory behaviour with mainly positive values before the maximum filling discharge is reached and mainly negative values after). When including representative profiles for the momentum correction coefficient, the observed variation of the bow-to-stern slope corresponds to the variation of the longitudinal force due to the combined effect of both the translatory wave and the momentum decrease effects.

Further research is recommended in order to verify whether the bow-to-stern slope obtained by solving the 1D SWE, with the momentum correction coefficient according to 'vul_sluis_impuls_straal_LVH.m', includes both the translatory wave and the momentum decrease effects. To that end, it is proposed to study the expression for the longitudinal force component due to the momentum decrease along the length of the vessel, as implemented in LOCKFILL and 'vul_sluis.m'. The obtained results with the for this master's thesis developped code 'Lock_Filling.m' can also be compared to the results obtained with LOCKFILL and 'vul_sluis.m'.

For the determination of representative profiles for the momentum correction coefficient, further research might also be useful due to the many assumptions inherent to the development of the code 'vul_sluis_impuls_straal_LVH.m'. For the most general case, this would mean research with respect to the description of the filling jet, for a lock chamber with a moored vessel, where the water volume is not at rest.

# References


[1] W. F. Molenaar, Hydraulic Structures: Locks, Course Notes, Delft: Delft University of Technology, 2011.

[2] Flanders Hydraulics Research, “Research on the influence of breaking logs on the flow pattern in locks with (filling) openings in the lock gate,” Flanders Hydraulics Research, 13 April 2016. [Online]. Available: http://www.watlab.be/en/research-on-the-influence-of-breaking-logs-on-the-flow-pattern-in-locks-with-filling-openings-in-the. [Accessed 17 August 2017].

[3] T. De Mulder, K. Verelst, J. B. Vercruysse, W. De Cock and M. Haegeman, “On hawser force criteria for navigation lock design: Case study of maritime locks in port of Antwerp,” *32nd PIANC Congress, 125th anniversary PIANC - setting the course,* no. 10 - 14 May 2010: PIANC MMX papers, pp. 1-19, 2010.

[4] Deltares, LOCKFILL: User & Technical Manual, Delft: Deltares, 2016.

[5] K. Verelst, T. De Mulder, L. Schindfessel, P. Peeters and F. Mostaert, “Numerieke modellering van sluisvulling via openingen in deuren: Deelrapport 1: Opmaak en eerste validatie van het programma vul_sluis,” Waterbouwkundig Laboratorium, Antwerpen, België, 2014.

[6] G. A. Schohl, User's Manual for LOCKSIM, Norris, Tennessee: TVA Engineering Laboratory, 1998.

[7] G. S. Stelling, “Speurwerk verslag S105: Rekenschema's voor de water- en scheepsbeweging in een schutsluis,” TOW, Delft, 1978.

[8] S. Roux, P. Roumieu, T. De Mulder, M. Vantorre, J. De Regge and J. Wong, “Determination of hawser forces using numerical and physical models for the third set of Panama locks studies,” *32nd PIANC Congress, 125th anniversary PIANC - setting the course,* no. 10 - 14 May 2010: PIANC MMX papers, pp. 1-15, 2010.

[9] T. De Mulder, Hydraulica I, Course Notes [in Dutch], Ghent: Ghent University, 2015.

[10] L. J. Mostertman, “Waves of long and short period,” in *Selected Aspects of Hydraulic Engineering, Liber Amicorum dedicated to Johannes Theodoor Thijsse, on occasion of his retirement as professor*, Delft, TU Delft, Section Hydraulic Engineering, 1963, pp. 151-168.

[11] T. De Mulder, *Modified Stelling (1978) approach to solve 1D Shallow Water Equations in a lock chamber. Documentation of Fortran code,* 2006.

[12] R. Szymkiewicz, “Oscillation-free solution of shallow water equations for non-staggered grid,” *Journal of Hydraulic Engineering,* no. 119(10), pp. 1118-1137, 1993.

[13] G. S. Stelling and S. A. Duinmeijer, “A staggered conservative scheme for every Froude number in rapidly varied shallow water flows,” *International journal for numerical methods in fluids,* no. 43(12), pp. 1329-1354, 2003.

[14] C. Hirsch, Numerical computation of internal and external flows, Brussel: Wiley, 1988.

[15] O. Gündüz, *Numerical modeling of flow and contaminant transport in rivers - Numerical solution of flow equations,* Atlanta, 2004.

[16] C. B. Vreugdenhil, Waterloopkundige berekeningen I, Course notes [in Dutch], Delft: TU Delft, 1979.

[17] L. Schindfessel and T. De Mulder, “Memo studieopdracht naar de berekening van debiet en impuls in het programma vul_sluis.m [in Dutch],” Hydraulics Laboratory, Dep. Civil Engineering, Ghent University, Ghent, 2017.

[18] A. Vrijburcht, “Het vulproces van een schutsluis met een langsvulsysteem: invloed translatiegolven, vulstraaleffekten en dichtheidsverschillen op de langskrachten. Verslag berekeningen.,” Delft Hydraulics Laboratory (Waterloopkundig Laboratorium), Delft, 1988.

[19] Wikipedia, “Hawser - Wikipedia,” Wikipedia, 13 June 2017. [Online]. Available: https://en.wikipedia.org/wiki/Hawser. [Accessed 18 August 2017].

# Appendix A – Dimensional Analysis 1D SWE

To get more insight with respect to the relative importance of the different terms in the momentum equation of the 1D SWE, a dimensional analysis is described in this appendix.

In [9] a dimensional analysis is carried out for the momentum equation written in the form[9]

$$\frac{\partial U}{\partial t} + U\frac{\partial U}{\partial x} = g\left(S_0 - S_f - \frac{\partial h}{\partial x}\right)$$

For the dimensional analysis, the bed slope $S_0$ is assumed to be equal to zero, and a wide rectangular cross section is assumed, so that the hydraulic radius R can be approximated by the water level h. The friction slope is expressed by applying a Chézy formulation. For these assumptions, the above momentum equation can be rewritten as

$$\frac{\partial U}{\partial t} + U\frac{\partial U}{\partial x} + g\frac{\partial h}{\partial x} + g\frac{U|U|}{C^2 h} = 0$$

From left to right, the different terms in this momentum equation represent the local acceleration, the advective acceleration, the pressure gradient and the bottom friction. Following the derivation and the notations adopted in [9], the dimensionless momentum equation becomes

$$\left(\frac{C^2 D^{0.5}}{g^{1.5}\, T\, Fr}\right)\frac{\partial U'}{\partial t'} + \left(\frac{C^2 D}{g\, L}\right)U'\frac{\partial U'}{\partial x'} + \left(\frac{C^2 D}{g\, Fr^2\, L}\right)\frac{\partial h'}{\partial x'} + \frac{U'|U'|}{h'} = 0$$

where the dimensionless dependent and independent variables are indicated with an accent. The coefficients in front of the different terms (between round brackets) represent the importance of these terms with respect to the bottom friction term.

The parameters D, L, T and Fr respectively represent the vertical length scale, the horizontal length scale, the time scale, and the Froude number. The Froude number is determined as

$$Fr = \frac{U_0}{\sqrt{gD}}$$

where $U_0$ represents the velocity scale. Representative values for these different scales are determined based on the studied Denderbelle lock (for filling the lock chamber without a moored vessel).

For the vertical length scale D, the average value of the initial and equilibrium water depth in the lock chamber is used, equal to about 5 m. For the horizontal length scale L, the wave length of the generated translatory waves is used, which corresponds to twice the lock chamber length $L_c$ for a lock

[9] Note that this momentum equation is equivalent to the one mentioned in paragraph 3 but is expressed for the cross sectional averaged velocity U and the water level deviation h as dependent variables.

chamber without a moored vessel, equal to 260 m. A representative value for the time scale T is then determined based on an estimate for the translatory wave period as

$$T = \frac{L}{c} \approx \frac{L}{\sqrt{gD}} = \frac{260\ m}{\sqrt{9.81\ \frac{m}{s^2} \cdot 5\ m}} = 37.12\ s \approx 40\ s$$

When filling the Denderbelle lock, tlhe Froude number varies as a function of time and as a function of the distance from the upstream lock gate. The Froude numbers are very low and are situated in the range [0.0012 ; 0.0265]. For the representative Froude number, a value of 0.03 is selected.

Finally the Chézy friction coefficient is also observed to vary slightly with time and with the distance from the upstream lock gate. The observed Chézy friction coefficients vary in the range [69.24 $m^{0.5}/s$ ; 70.99 $m^{0.5}/s$], and a value of 70 $m^{0.5}/s$ is used for the calculations.

The coefficients representing the relative importance of the local acceleration, the advective acceleration, and the pressure gradient terms with respect to the bottom friction can then respectively be calculated as

$$\left(\frac{C^2 D^{0.5}}{g^{1.5}\ T\ Fr}\right) = 297.16 \approx O(10^2)$$

$$\left(\frac{C^2 D}{g\ L}\right) = 9.61 \approx O(10^1)$$

$$\left(\frac{C^2 D}{g\ Fr^2\ L}\right) = 10\ 672.87 \approx O(10^4)$$

From the order of magnitudes for these coefficients, it is concluded that the pressure gradient term and the local acceleration term are the most important terms. The advective acceleration and the bottom friction terms will be of lesser importance.

# Appendix B – Modified Stelling (1978) Method

In this appendix, the main sections and applied formulae for programming the modified Stelling (1978) method in the MATLAB script 'Lock_Filling.m' are described.

## B.1. Definition of the Grid

As mentioned in paragraph 4.1, the grid for the modified Stelling (1978) method is staggered in space. Based on the discharge boundary conditions at both the upstream and the downstream lock gates, the following formulae are derived to determine the number of discharge and water level nodes, and their distance x from the upstream lock gate.

$$x_Q(j) = (2j - 2)\Delta x$$

and

$$x_h(j) = (2j - 1)\Delta x$$

Since $x_Q(N_Q)$ should be equal to the lock chamber length $L_c$, the number of discharge nodes $N_Q$ is determined as

$$N_Q = round\left(\frac{L_{c,0}}{2\Delta x} + 1\right)$$

The subscript 0 indicates that the originally inputted lock chamber length is meant. The number of water level nodes is equal to

$$N_h = round\left(\frac{L_{c,0}}{2\Delta x}\right) = N_Q - 1$$

If the inputted lock chamber length $L_{c,0}$ is not compatible with the selected spatial step Δx, the actual lock chamber length for the simulation will be equal to

$$L_c = 2\Delta x N_h$$

The locations of the discharge and the water level nodes in metre from the upstream lock gate, are stored in the column vectors $x_Q$ and $x_h$ respectively.

## B.2. Position Ship in Grid

If the flag 'i_ship' is set to one, a ship is present in the lock chamber. This ship does not necessarily have dimensions compatible with the grid. To that end, attention is paid to the way the ship is positioned in the lock chamber.

The input parameter 'i_adjust' determines whether the position of the ship is adjusted to let the midship's cross section coincide with the closest water level node. If 'i_adjust' is equal to zero, the position of the ship is not adjusted. If 'i_adjust' is equal to one, the position of the ship is adjusted so that the midship's cross section coincides with the closest water level node. It is mentioned here that for the rigid ship approach, 'i_adjust' should be equal to one, since the integrals expressed for the determination of s and γ will not be equal to zero initially if the midship cross section does not coincide with a water level node.

The index for the position of the midship's cross section is determined based on the expression for the locations of the water level nodes as

$$i_M = round\left(\frac{x_{M,0}}{2\Delta x} + 0.5\right)$$

If 'i_adjust' is equal to zero, the final position of the midship's cross section is equal to

$$x_M = x_{M,0}$$

If 'i_adjust' is equal to one, the new position of the midship's cross section is equal to

$$x_M = (2i_M - 1)\Delta x$$

The new position of the bow and the stern of the ship are respectively determined as

$$x_{bow} = x_M - \frac{L_s}{2}$$

and

$$x_{stern} = x_M + \frac{L_s}{2}$$

To define the section where the ship is present, indices have to be determined to represent the location of the bow and the stern of the ship. In this master's thesis the bow and the stern of the ship are assumed to reach up until the closest water level node, and the corresponding indices respectively become

$$i_{bow} = round\left(\frac{x_{bow}}{2\Delta x} + 0.5\right)$$

$$i_{stern} = round\left(\frac{x_{stern}}{2\Delta x} + 0.5\right)$$

The width and the draft of the ship are then defined at each water level node and stored in the column vectors $B_s(x)$ and $T_s(x)$ respectively. The following expressions apply

$$B_s(x) = \begin{cases} 0, & i < i_{bow} \\ B_s, & i_{bow} \leq i \leq i_{stern} \\ 0, & i \geq i_{stern} \end{cases}$$

$$T_s(x) = \begin{cases} 0, & i < i_{bow} \\ T_s, & i_{bow} \leq i \leq i_{stern} \\ 0, & i \geq i_{stern} \end{cases}$$

It is noted that the column vectors $B_s(x)$ and $T_s(x)$ reflect the different sections in a lock chamber with a moored vessel, as displayed in Figure 4.

## B.3. Runge-Kutta (Determination of the Right-Hand Side)

As described in paragraph 4.3, the Runge-Kutta time-stepping method is applied to a system of discretized (partial) differential equation written in the form

$$\frac{dY}{dt} = F(t, Y)$$

The Runge-Kutta time-stepping method is described in paragraph 4.3. In this paragraph, the discretized systems of partial differential equations are presented for both a lock chamber with and without a moored vessel, and for the flexible and the rigid ship approaches. The geometrical characteristics are not repeated here. It is however noted that the geometrical characteristics are only determined at the water level nodes. Linear interpolation is then applied to determine the geometrical characteristics at the discharge nodes.

To clearly display the applicable systems of discretized (partial) differential equations, the pages containing these equations are turned.

### B.3.1. Lock Chamber Without Moored Vessel

For the lock chamber without a moored vessel, the system of discretized partial differential equations becomes

$$\begin{cases} \left(\frac{\partial h}{\partial t}\right)_j = \frac{-1}{B_c}\frac{Q_{j+1}-Q_j}{2\Delta x} \\ \left(\frac{\partial Q}{\partial t}\right)_j = \frac{-1}{8\Delta x}\left[\frac{\beta_j\left(Q_{j+1}+Q_j\right)^2}{A_j} - \frac{\beta_{j-1}\left(Q_j+Q_{j-1}\right)^2}{A_{j-1}}\right] - g\frac{A_j+A_{j-1}}{2}\frac{h_j-h_{j-1}}{2\Delta x} + g\frac{Q_j|Q_j|}{\left(\frac{C_j+C_{j-1}}{2}\right)^2\left(\frac{A_j+A_{j-1}}{2}\right)\left(\frac{R_j+R_{j-1}}{2}\right)} \end{cases}$$

It is kept in mind that the momentum correction coefficient β, the wet cross sectional area A, the hydraulic radius R and the Chézy friction coefficient are only determined at the water level nodes.

### B.3.2. Lock Chamber With Moored Vessel

For the situation where a vessel is moored in the lock chamber, two different approaches are implemented to model this vessel as described in paragraph 3.1.2. The same subdivision is made here.

#### B.3.2.1. Flexible Ship Method

When the moored vessel is modelled according to the flexible ship method, the applicable system of discretized (partial) differential equations becomes

$$\begin{cases} \left(\frac{\partial h}{\partial t}\right)_j = \frac{-1}{B_c}\frac{Q_{j+1}-Q_j}{2\Delta x} \\ \left(\frac{\partial Q}{\partial t}\right)_j = \frac{-1}{8\Delta x}\left[\frac{\beta_j\left(Q_{j+1}+Q_j\right)^2}{A_j} - \frac{\beta_{j-1}\left(Q_j+Q_{j-1}\right)^2}{A_{j-1}}\right] - g\frac{A_j+A_{j-1}}{2}\frac{h_j-h_{j-1}}{2\Delta x} + g\frac{Q_j|Q_j|}{\left(\frac{C_j+C_{j-1}}{2}\right)^2\left(\frac{A_j+A_{j-1}}{2}\right)\left(\frac{R_j+R_{j-1}}{2}\right)} \end{cases}$$

This is the same system of discretized equations as for the lock chamber without a moored vessel, and was repeated to provide a complete overview. The presence of the ship becomes clear from the determination of the geometrical characteristics as described in paragraph 3.1.2.1.

### B.3.2.2. Rigid Ship Approach

When the moored vessel is modelled according to the rigid ship method, the applicable system of discretized (partial) differential equations becomes

$$
\begin{cases}
\left(\frac{\partial h}{\partial t}\right)_j = \frac{-1}{B_c - B_s}\frac{Q_{j+1} - Q_j}{2\Delta x} - g\frac{B_s}{B_c - B_s}\alpha - \frac{B_s}{B_c - B_s}(x_h(j) - x_M)\beta \\
\left(\frac{\partial Q}{\partial t}\right)_j = \frac{-1}{8\Delta x}\left[\frac{\beta_j\left(Q_{j+1} + Q_j\right)^2}{A_j} - \frac{\beta_{j-1}\left(Q_j + Q_{j-1}\right)^2}{A_{j-1}}\right] - g\frac{A_j + A_{j-1}}{2}\frac{h_j - h_{j-1}}{2\Delta x} + g\frac{Q_j|Q_j|}{\left(\frac{C_j + C_{j-1}}{2}\right)^2\left(\frac{A_j + A_{j-1}}{2}\right)\left(\frac{R_j + R_{j-1}}{2}\right)} \\
\frac{d\alpha_1}{dt} = -\frac{2gB_s}{V_s}\left(\frac{L_s}{2}\right)s + \frac{gB_s}{V_s}integral\_h \\
\frac{d\alpha_2}{dt} = -\frac{2gB_s}{V_s}\left(\frac{L_s}{2}\right)\gamma + \frac{3gB_s}{V_s\left(\frac{L_s}{2}\right)^2}integral\_x\_h \\
\frac{ds}{dt} = \alpha_1 \\
\frac{d\gamma}{dt} = \alpha_2
\end{cases}
$$

It is repeated here that for the rigid ship method, the continuity equation contains two additional terms to account for the sinkage s and the pitch of the ship. To determine these two unkown variables, two extra second order ordinary differential equations have to be solved. These second order ordinary differential equations are rewritten as first order ordinary differential equations by introducing the auxiliary variables $\alpha_1$ and $\alpha_2$.

The terms 'integral_h' and 'integral_x_h' denote the numerical approximations of the integrals occuring in the differential equations for the determination of respectively the auxiliary variables $\alpha_1$ and $\alpha_2$. The determination of these integrals depends on the position of the vessel in the grid. One of four possible situations is displayed in Figure 30. For this situation the closest water level node to the bow is located in the section with the ship, and the closest water level node to the stern is located outside the section with the ship. For the three other situations, the calculation procedure is analogous to the one described below.

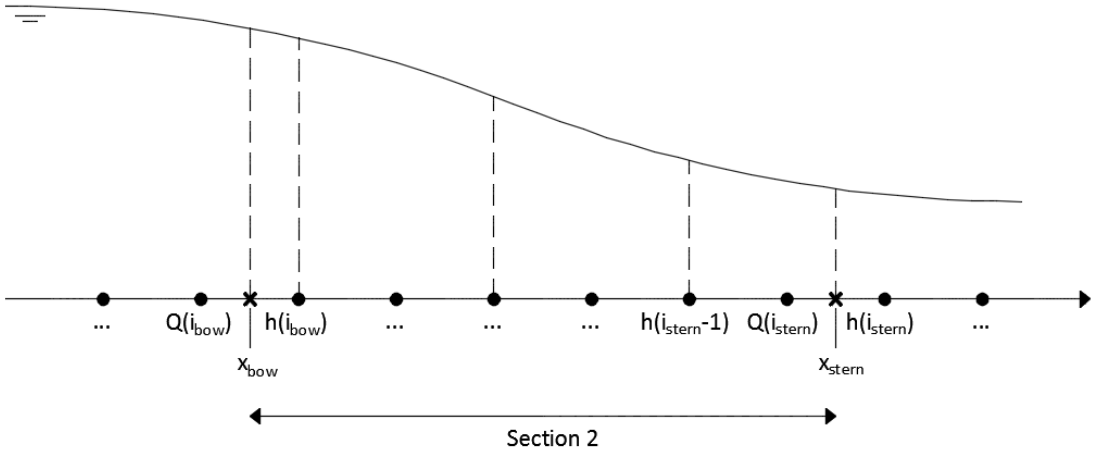


**Figure 30 – Possible position of the ship in the grid for the modified Stelling (1978) method**

By applying Simpson's rule, the value for the parameter 'integral_h' is determined as

$$\int_{x_{bow}}^{x_{stern}} h dx \approx \frac{h_{bow} + h(i_{bow})}{2}\left(x_h(i_{bow}) - x_{bow}\right) + \sum_{j=i_{bow}}^{i_{stern}-2} \frac{h(j) + h(j+1)}{2} 2\Delta x + \frac{h(i_{stern}-1) + h_{stern}}{2}\left(x_{stern} - x_h(i_{stern}-1)\right)$$

The values for the water level at the bow ($h_{bow}$) and the stern ($h_{stern}$) of the vessel are determined through linear interpolation. By taking into account the distance ($x$-$x_M$), the value for the parameter 'integral_x_h' is calculated analogously.

## B.4. Output

For studying the results afterwards, the important calculation results are stored in matrices.

For the water levels, the matrix 'h_x_t_RK' with a number of rows equal to the number of time steps $N_t$, and a number of columns equal to the number of water level nodes $N_h$ is created. The same is done for the discharges, stored in 'Q_x_t_RK', and the momentum correction coefficient β, stored in 'BetaM_x_t_RK'.

When a ship is modelled according to the rigid ship method, the additional matrix 'Ship_Output_RK' contains the values for the the auxiliary variables $\alpha_1$ and $\alpha_2$, and the sinkage s and pitch γ of the moored vessel as a function of time.

For each time step, the difference between the equilibrium water level $h_e$ and the average water level in the lock chamber is also determined. When the absolute value of this difference is smaller than 0.1 respectively 0.001, levelling of the lock chamber is said to have occurred according to criterion 1 and criterion 2. The corresponding levelling times are stored in the parameters '$t_{niv,1}$' and '$t_{niv,2}$'.

# Appendix C – Preissmann Method

In this appendix, the main sections and applied formulae for programming the Preissmann method in the MATLAB script 'Lock_Filling.m' are described.

## C.1. Definition of the Grid

As described in paragraph 5.1, a collocated grid is used for the Preissmann method. The definition of this grid is more straightforward than the definition of the space staggered grid for the modified Stelling (1978) method.

The number of nodes $N_x$ is determined as

$$N_x = round\left(\frac{L_{c,0}}{\Delta x} + 1\right)$$

The round() function is again applied, since the inputted lock chamber length $L_{c,0}$ is not necessarily compatible with the selected spatial step Δx. Therefore the lock chamber length used throughout the calculations is equal to

$$L_c = (N_x - 1)\Delta x$$

## C.2. Position Ship in Grid

The remarks with respect to the parameter 'i_adjust' described in paragraph B.2. are also applicable here.

The index of the position of the midship's cross section is determined as

$$i_M = round\left(\frac{x_{M,0}}{\Delta x} + 1.0\right)$$

If 'i_adjust' is equal to zero, the final position of the midship's cross section is equal to

$$x_M = x_{M,0}$$

If 'i_adjust' is equal to one, the new position of the midship's cross section is equal to

$$x_M = (i_M - 1)\Delta x$$

The new position of the bow and the stern of the ship respectively become

$$x_{bow} = x_M - \frac{L_s}{2}$$

and

$$x_{stern} = x_M + \frac{L_s}{2}$$

To define the section where the ship is present, indices have to be determined to represent the location of the bow and the stern of the ship. In this master's thesis the bow and the stern of the ship are assumed to reach up until the closest node, and the corresponding indices respectively become

$$i_{bow} = round\left(\frac{x_{bow}}{\Delta x} + 1.0\right)$$

$$i_{stern} = round\left(\frac{x_{stern}}{\Delta x} + 1.0\right)$$

The width and the draft of the ship are now defined at each node and stored in the column vectors $B_s(x)$ and $T_s(x)$ respectively. The following expressions apply

$$B_s(x) = \begin{cases} 0, & i < i_{bow} \\ B_s, & i_{bow} \leq i \leq i_{stern} \\ 0, & i \geq i_{stern} \end{cases}$$

$$T_s(x) = \begin{cases} 0, & i < i_{bow} \\ T_s, & i_{bow} \leq i \leq i_{stern} \\ 0, & i \geq i_{stern} \end{cases}$$

It is noted that the column vectors $B_s(x)$ and $T_s(x)$ again reflect the different sections in a lock chamber with a moored vessel, as displayed in Figure 4.

## C.3. Discretized System of Equations

In this paragraph, the discretized systems of equations for the Preissmann method are presented. To provide a clear overview, the pages containing these equations are again tilted.

### C.3.1. Lock Chamber Without Moored Vessel

For the lock chamber without a moored vessel, the system of discretized partial differential equations becomes

$$\begin{cases} \frac{B_c \Delta x}{2\Delta t}\left(h_j^{n+1} - h_j^n + h_{j-1}^{n+1} - h_{j-1}^n\right) + \theta\left(Q_j^{n+1} - Q_{j-1}^{n+1}\right) + (1-\theta)\left(Q_j^n - Q_{j-1}^n\right) = 0 \\ \frac{\Delta x}{2\Delta t}\left(Q_j^{n+1} - Q_j^n + Q_{j-1}^{n+1} - Q_{j-1}^n\right) + \theta\left[\left(\frac{\beta Q^2}{A}\right)_j^{n+1} - \left(\frac{\beta Q^2}{A}\right)_{j-1}^{n+1} + gA_{j-\frac{1}{2}}^{n+1}\left(h_j^{n+1} - h_{j-1}^{n+1}\right) + g\Delta x\left(\frac{Q|Q|}{C^2AR}\right)_{j-\frac{1}{2}}^{n+1}\right] + (1-\theta)\left[\left(\frac{\beta Q^2}{A}\right)_j^{n} - \left(\frac{\beta Q^2}{A}\right)_{j-1}^{n} + gA_{j-\frac{1}{2}}^{n}\left(h_j^{n} - h_{j-1}^{n}\right) + g\Delta x\left(\frac{Q|Q|}{C^2AR}\right)_{j-\frac{1}{2}}^{n}\right] = 0 \end{cases}$$

The subscripts denote the node under consideration, the superscripts denote whether the known values at the current time nΔt, or the unkown values at the time (n+1)Δt are meant.

The index j-1/2 denotes that the indicated quantities are specified at the centre of the cell for which the momentum equation is expressed. For example, the wet cross sectional area A at the centre of the cell is determined as

$$A_{j-\frac{1}{2}} = \frac{A_{j-1} + A_j}{2}$$

The other cell centre quantities are determined analogously.

### C.3.2. Lock Chamber With Moored Vessel

For the situation where a vessel is moored in the lock chamber, two different approaches are implemented to model this vessel as described in paragraph 3.1.2. The same subdivision is made here.

#### C.3.2.1. Flexible Ship Method

When the moored vessel is modelled according to the flexible ship method, the applicable system of discretized (partial) differential equations becomes

$$\begin{cases} \dfrac{B_c\Delta x}{2\Delta t}\left(h_j^{n+1}-h_j^n+h_{j-1}^{n+1}-h_{j-1}^n\right)+\theta\left(Q_j^{n+1}-Q_{j-1}^{n+1}\right)+(1-\theta)\left(Q_j^n-Q_{j-1}^n\right)=0 \\ \dfrac{\Delta x}{2\Delta t}\left(Q_j^{n+1}-Q_j^n+Q_{j-1}^{n+1}-Q_{j-1}^n\right)+\theta\left[\left(\dfrac{\beta Q^2}{A}\right)_j^{n+1}-\left(\dfrac{\beta Q^2}{A}\right)_{j-1}^{n+1}+gA_{j-\frac{1}{2}}^{n+1}\left(h_j^{n+1}-h_{j-1}^{n+1}\right)+g\Delta x\left(\dfrac{Q|Q|}{C^2AR}\right)_{j-\frac{1}{2}}^{n+1}\right]+(1-\theta)\left[\left(\dfrac{\beta Q^2}{A}\right)_j^{n}-\left(\dfrac{\beta Q^2}{A}\right)_{j-1}^{n}+gA_{j-\frac{1}{2}}^{n}\left(h_j^{n}-h_{j-1}^{n}\right)+g\Delta x\left(\dfrac{Q|Q|}{C^2AR}\right)_{j-\frac{1}{2}}^{n}\right]=0 \end{cases}$$

This is the same system of discretized equations as for the lock chamber without a moored vessel. This system of equations is repeated here to provide a complete overview. The presence of the flexible ship becomes clear from the determination of the geometrical characteristics as described in paragraph 3.1.2.1.

### C.3.2.2. Rigid Ship Method

When the moored vessel is modelled according to the rigid ship method, the applicable system of discretized (partial) differential equations becomes

$$\begin{cases} \dfrac{(B_c-B_s)\Delta x}{2\Delta t}\left(h_j^{n+1}-h_j^n+h_{j-1}^{n+1}-h_{j-1}^n\right)+\theta\left(Q_j^{n+1}-Q_{j-1}^{n+1}+B_s\Delta x\alpha^{n+1}+B_s\Delta x\left(\dfrac{x_j+x_{j-1}}{2}-x_M\right)\beta^{n+1}\right)+(1-\theta)\left(Q_j^n-Q_{j-1}^nB_s(x)\Delta x\alpha^n+B_s(x)\Delta x\left(\dfrac{x_j+x_{j-1}}{2}-x_M\right)\beta^n\right)=0 \\ \dfrac{\Delta x}{2\Delta t}\left(Q_j^{n+1}-Q_j^n+Q_{j-1}^{n+1}-Q_{j-1}^n\right)+\theta\left[\left(\dfrac{\beta Q^2}{A}\right)_j^{n+1}-\left(\dfrac{\beta Q^2}{A}\right)_{j-1}^{n+1}+gA_{j-\frac{1}{2}}^{n+1}\left(h_j^{n+1}-h_{j-1}^{n+1}\right)+g\Delta x\left(\dfrac{Q|Q|}{C^2AR}\right)_{j-\frac{1}{2}}^{n+1}\right]+(1-\theta)\left[\left(\dfrac{\beta Q^2}{A}\right)_j^{n}-\left(\dfrac{\beta Q^2}{A}\right)_{j-1}^{n}+gA_{j-\frac{1}{2}}^{n}\left(h_j^{n}-h_{j-1}^{n}\right)+g\Delta x\left(\dfrac{Q|Q|}{C^2AR}\right)_{j-\frac{1}{2}}^{n}\right]=0 \\ \dfrac{\alpha^{n+1}-\alpha^n}{\Delta t}+\theta\left[\dfrac{gB_sL_s}{V_s}s^{n+1}-\dfrac{gB_s}{V_s}integral\_x^{n+1}\right]+(1-\theta)\left[\dfrac{gB_sL_s}{V_s}s^{n}-\dfrac{gB_s}{V_s}integral\_x^{n}\right]=0 \\ \dfrac{\beta^{n+1}-\beta^n}{\Delta t}+\theta\left[\dfrac{gB_sL_s}{V_s}\gamma^{n+1}-\dfrac{12gB_s}{V_sL_s^2}integral\_x\_h^{n+1}\right]+(1-\theta)\left[\dfrac{gB_sL_s}{V_s}\gamma^{n}-\dfrac{12gB_s}{V_sL_s^2}integral\_x\_h^{n}\right]=0 \\ s^{n+1}-s^n-\theta\Delta t\alpha^{n+1}-(1-\theta)\Delta t\alpha^n=0 \\ \gamma^{n+1}-\gamma^n-\theta\Delta t\beta^{n+1}-(1-\theta)\Delta t\beta^n=0 \end{cases}$$

For the determination of the parameters 'integral_x' and 'integral_x_h' the same calculation procedure as outlined in paragraph B.3.2.2. is followed. It is noted that due to the weighting factor θ in time, these integrals have to be determined at the previous time nΔt as well as at the considered time (n+1)Δt.

## C.4. Output

For studying the results afterwards, the important calculation results are stored in matrices.

For the water levels, the matrix 'h_x_t_Preiss' with a number of rows equal to the number of time steps $N_t$, and a number of columns equal to the number of nodes $N_x$ is created. The same is done for the discharges, stored in 'Q_x_t_Preiss', and the momentum correction coefficient β, stored in 'BetaM_x_t_Preiss'.

When a ship is modelled according to the rigid ship method, the additional matrix 'Ship_Output_Preiss' contains the values for the the auxiliary variables $\alpha_1$ and $\alpha_2$, and the sinkage s and pitch γ of the moored vessel as a function of time.

The levelling times stored in '$t_{niv,1}$' and '$t_{niv,2}$' are determined based on the same two criteria as described in paragraph B.4.

# Appendix D – Results Adjusted Boundary Conditions Modified Stelling (1978)

Based on the irregular behaviour of the filling discharge and the bow-to-stern slope after $t_{niv,2}$ has been reached (for the larger time steps), the upstream discharge boundary condition is adjusted in order to verify whether this might resolve the observed results.

Originally, the difference between the equilibrium water level $h_e$, and the water level just downstream of the upstream lock gate is used to determine the head as a function of time. For this appendix, the upstream discharge boundary condition is adjusted by determining the time evolution of the head as the difference between the equilibrium water level $h_e$ and the average water level in the lock chamber.

The results for the filling discharge, the head, and the bow-to-stern slope as a function of time are respectively displayed in Figure 31, Figure 32 and Figure 33. These quantities are made dimensionless in the same manner as in paragraph 8.1.1.

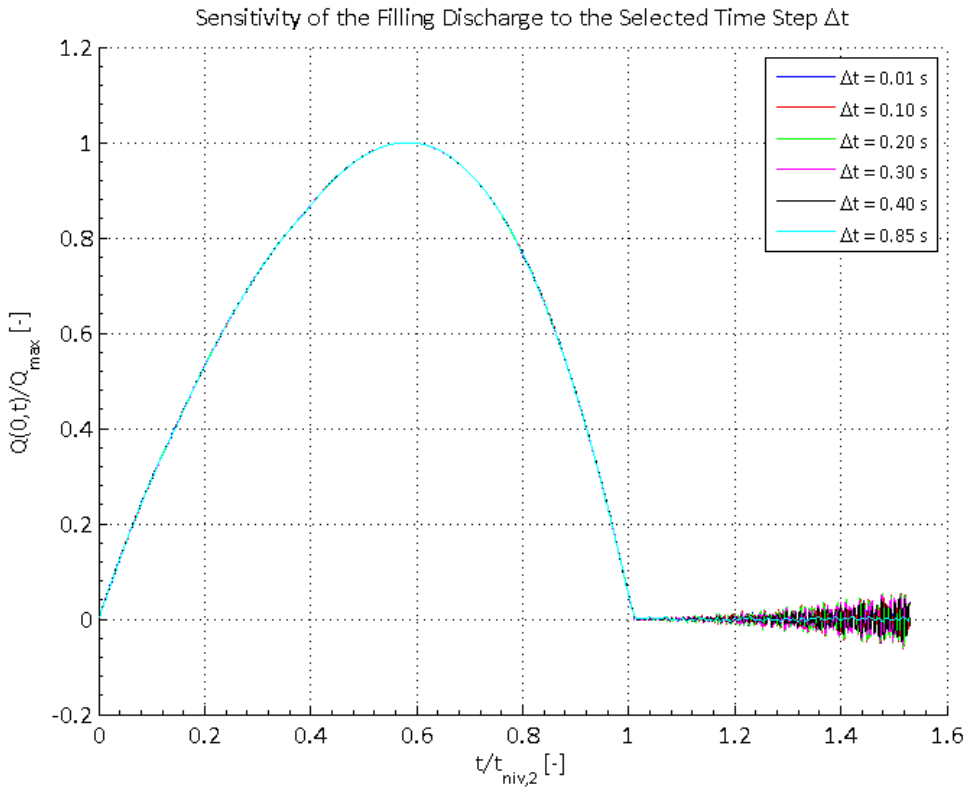


**Figure 31 – Sensitivity of the filling discharge to the time step Δt for the adjusted upstream boundary condition**

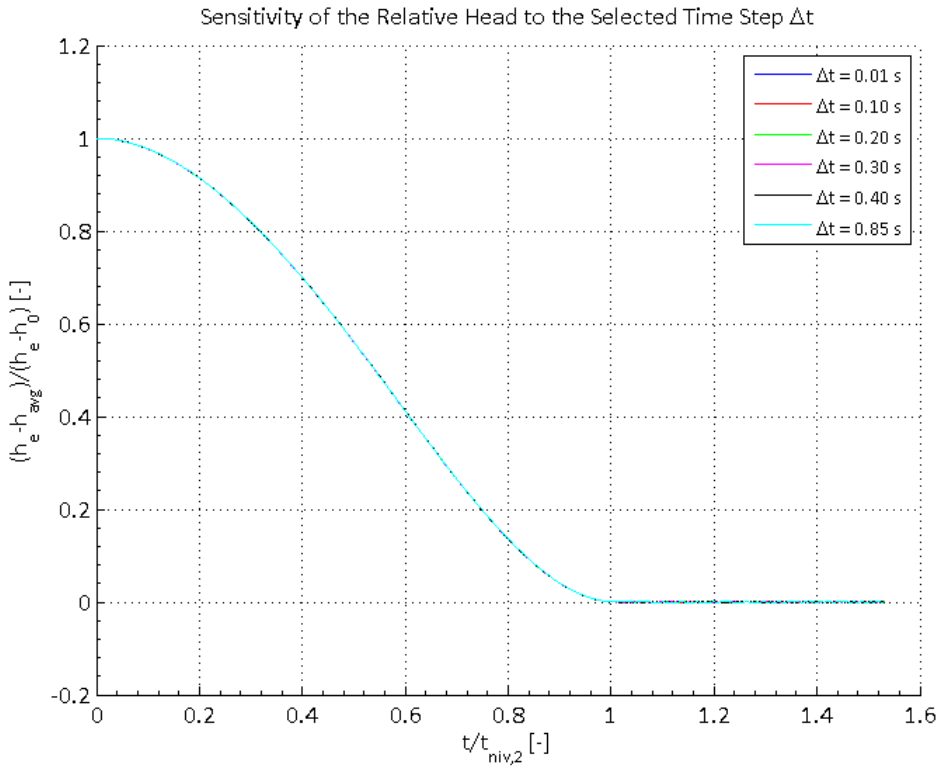


**Figure 32 – Sensitivity of the relative head to the time step Δt for the adjusted upstream boundary condition**

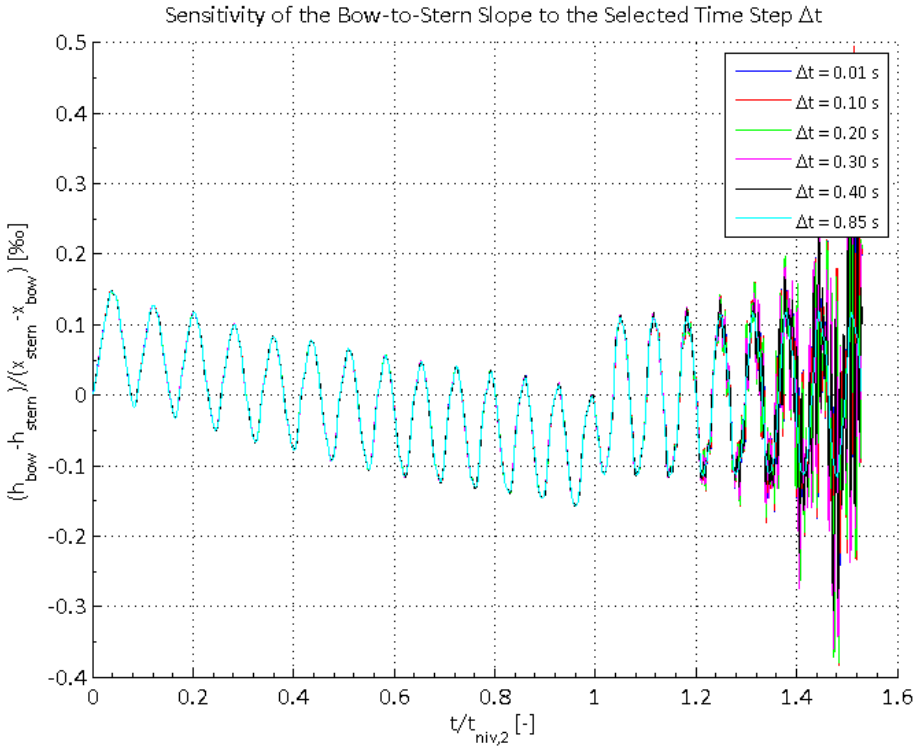


**Figure 33 – Sensitivity of the bow-to-stern slope to the time step Δt for the adjusted upstream boundary condition**

From Figure 31 and Figure 33, it is clear that after $t_{niv,2}$ has been reached, the results still display an oscillating behaviour, even for the first two simulations (lowest time steps). Furthermore, the oscillations are observed to grow for longer calculation times, which typically is an indication of the calculations becoming unstable.

It is concluded that adjusting the upstream discharge boundary condition does not resolve the problems described in paragraph 8.1.1. For the original definition of the boundary conditions, selecting a lower time step Δt resolves the problem, and this is therefore done in this master's thesis.